iScience

CellPress
OPEN ACCESS

Review

Flexible strategy of epitaxial oxide thin films

Jijie Huang[1,2,3,*] and Weijin Chen[1,2,3]

SUMMARY

Applying functional oxide thin films to flexible devices is of great interests within the rapid development of information technology. The challenges involve the contradiction between the high-temperature growth of high-quality oxide films and low melting point of the flexible supports. This review summarizes the developed methods to fabricate high-quality flexible oxide thin films with novel functionalities and applications. We start from the fabrication methods, e.g. direct growth on flexible buffered metal foils and layered mica, etching and transfer approach, as well as remote epitaxy technique. Then, various functionalities in flexible oxide films will be introduced, specifically, owing to the mechanical flexibility, some unique properties can be induced in flexible oxide films. Taking the advantages of the excellent physical properties, the flexible oxide films have been employed in various devices. Finally, future perspectives in this research field will be proposed to further develop this field from fabrication, functionality to device.

INTRODUCTION

Complex oxide thin films have attracted extensive research interests, owing to their rich functionalities and great potential in electronic and spintronic devices (Lorenz et al., 2016). The electron, orbital, spin, and lattice degrees of freedom in functional oxides lead to exotic physical properties and multi-field coupling between them, which involves multiferroicity, ferroelectricity, magnetism, magnetoresistance, plasmonics, superconductivity, etc. (Wang et al., 2003; Dawber et al., 2005; Huang and Wang, 2017; Kacedon et al., 1997). Furthermore, the development of oxide-based nanocomposite thin film composing of two or more phases in one single layer extends the modulation of the physical properties in oxide thin films, as well as the discovery of new physical phenomenon (Huang et al., 2017, 2021e; MacManus-Driscoll, 2010). Because of the tunable functionalities and rich oxide material selection, oxide thin films have been applied in various device demonstrations, such as resistive switching memory, gas sensor, Li-ion battery, optical applications, soft bioelectronics, wearable tactile sensors, soft robotics, etc. (Acharya et al., 2016; Liu et al., 2015, 2022a, 2022b; Qi et al., 2018; Sando et al., 2018; Guo and Ding, 2021; Roels et al., 2022).

In another side, flexible or wearable devices play more and more important role in today's electronic world, which offers advantages over conventional Si-based solid electronics (Liu et al., 2017a, 2017b; Bao and Chen, 2016). Flexible/wearable devices have been employed in the new generation technologies, such as light-weight personal electronics, sensors for human health monitoring, as well as Internet of Things (IoT) applications (Yamamoto et al., 2016; Son et al., 2014; Gao et al., 2016). The flexible devices mainly rely on the mechanically flexible organic materials, which could maintain physical properties under bending condition without damage. Taking the advantages of the multi-functional oxides, it is highly desirable to achieve oxide thin films on flexible substrates for flexible electronics. However, flexible organic materials exhibit relatively low melting point (usually lower than 300°C), while high-quality or epitaxial oxide thin films need high-temperature deposition process (usually higher than 600°C). Such contradiction makes it very challenging to realize flexible oxide thin films with high quality.

Fortunately, tremendous efforts have been devoted to obtain high-quality flexible oxide thin films, and effective approaches have been developed. In general, it can be divided into two major directions, refers to direct growth and transfer method. The former can be realized by either finding flexible substrates with high melting point or developing low-temperature growth method. The basic idea of the latter is to deposit oxide thin films on soluble substrates or buffer layers first, and then remove the sacrificial substrates or buffers to obtain freestanding oxide thin films; such freestanding films can be transferred onto flexible substrates. In this review, we will give more details on how to achieve high-quality flexible oxide thin films by

[1]School of Materials, Shenzhen Campus of Sun Yat-sen University, Shenzhen 518107, China

[2]Guangdong Provincial Key Laboratory of Magnetoelectric Physics and Devices, School of Physics, Sun Yat-sen University, Guangzhou 510275, China

[3]Centre for Physical Mechanics and Biophysics, School of Physics, Sun Yat-sen University, Guangzhou 510275, China

*Correspondence: haungjj83@mail.sysu.edu.cn

https://doi.org/10.1016/j.isci.2022.105041

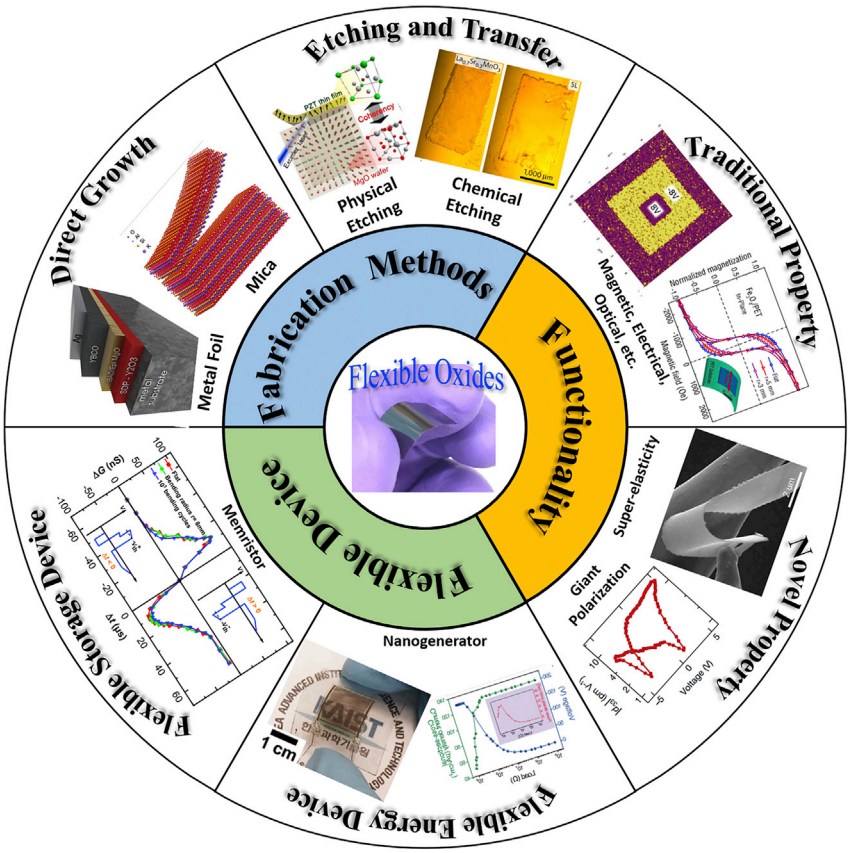

Figure 1. Summary of the fabrication methods, functionality, and flexible device
Overview of contents in this review on the flexible strategy of functional oxide thin films for wearable devices.

discussing successful attempts, and the advantages and disadvantages of each method will be compared. Then, different functionalities of the reported flexible oxide thin films will be discussed, and their applications in flexible devices will also be demonstrated. Lastly, perspectives will be proposed on future works in the research field of flexible oxide thin films with different functionalities. Figure 1 presents the overview of this research field, which will be discussed in detail in this review.

FABRICATION OF HIGH-QUALITY FLEXIBLE OXIDE THIN FILMS

Direct growth on flexible substrates

Direct growth on flexible metal foil

Metal foil or metal tape serves as a great platform as a flexible substrate for high-temperature process. One typical example is the fabrication of $YBa_2Cu_3O_{7-x}$ (YBCO) superconductor-coated conductors, which produces epitaxial YBCO superconducting thin film on metal tape. The flexible metal tape could be obtained by standard thermo-mechanical processing with strong biaxial texture and smooth surface, which provides appropriate crystallinity and surface condition for the following oxide thin film growth (Goyal et al., 1996a, 1996b). Even though, buffer layers are always required before growing YBCO, and two main technologies have been developed in the manufacture of coated-conductor tapes, namely rolling-assisted biaxially textured substrate (RABiTS) and ion-beam-assisted deposition (IBAD), as shown in Figure 2A (Norton et al., 1998; Foltyn et al., 2007).

Different epitaxial buffer layers have been achieved, typical materials include Y_2O_3-stabilized ZrO_2 (YSZ) (List et al., 1998; Ma et al., 2002; Jeong et al., 1998), CeO_2 (Ma et al., 2002; Goyal et al., 1996a, 1996b), Y_2O_3 (Shi et al., 2005; Fabbri et al., 2000), MgO (Matiasa and Hammond, 2012), multilayers (Tomov et al., 2002; Xue et al., 2016; Xiong et al., 2010), etc. For example, Xiong et al. developed $LaMnO_3$/TiN multi-buffer layers on electropolished Hastelloy tape (rms ~0.8 nm) for superconducting YBCO thin film growth

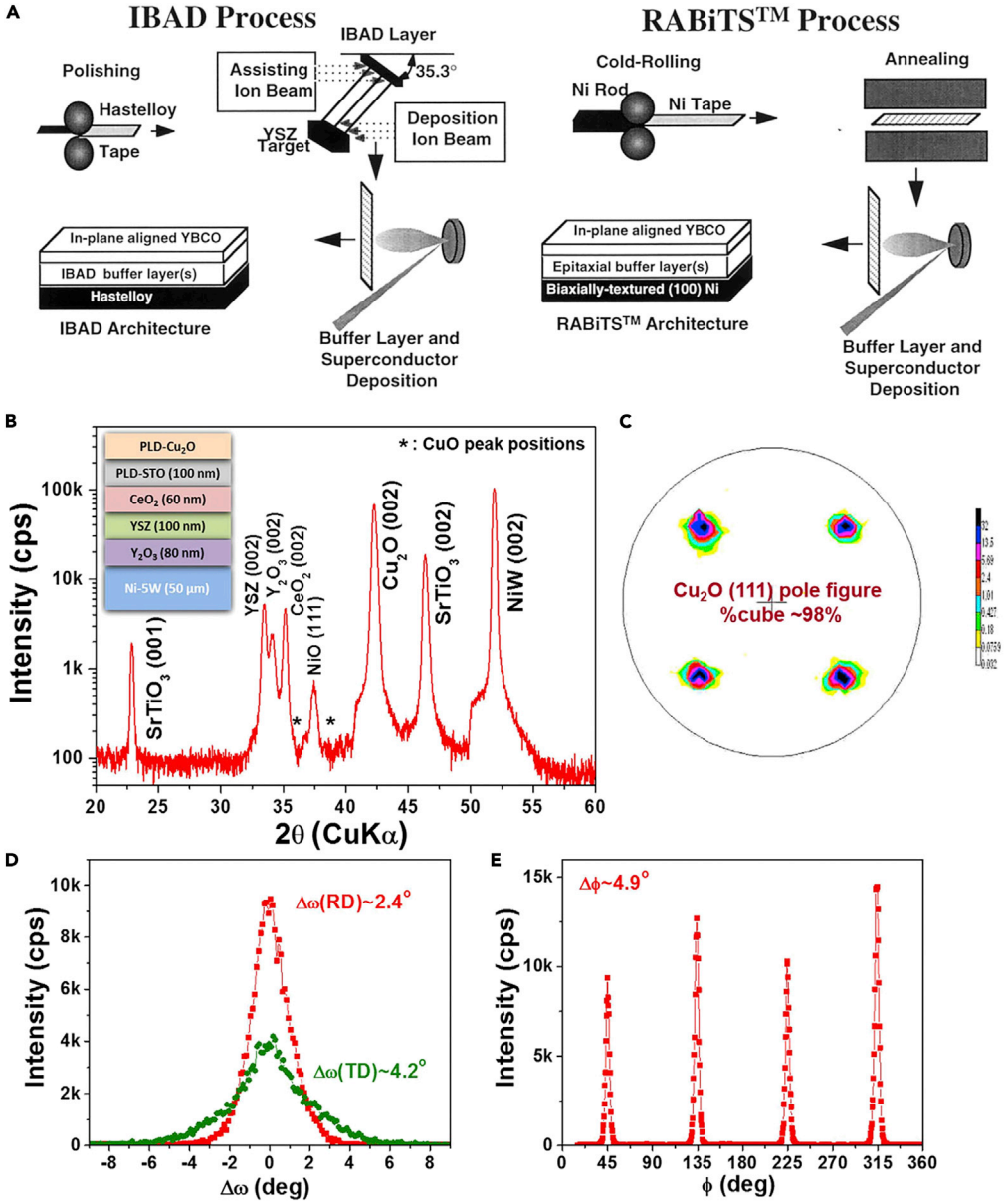

Figure 2. Direct growth of oxide thin films on flexible metal foils

(A) Schematic illustration of the IBAD and RABiTS processes to obtain buffered metal tapes for fabricating YBCO-coated conductors (Norton et al., 1998). Reprinted with permission from Elsevier.

(B) θ-2θ XRD scan the Cu_2O film grown on STO/CeO_2/YSZ/Y_2O_3 buffered Ni-W substrate, Inset shows the schematic illustration of the multilayer architecture; (C) (111) pole figure, (D) (002) ω-scans for both rolling (φ = 0°) and transverse (φ = 90°) directions, and (E) (111) φ-scan for the Cu_2O film (Wee et al., 2015). Reprinted under Creative Commons License https://creativecommons.org/licenses/by/4.0/.

(Xiong et al., 2010). Here, TiN (~10 nm) was first deposited using IBAD, followed by $LaMnO_3$ (~120 nm) growth by pulsed laser deposition. With such buffer stacks, epitaxial YBCO thin film was obtained with excellent superconducting properties, i.e. transition temperature (T_c) of 89.5 K, self-field critical current density (J_c) of 1.2 MA/cm^2 at 75.5 K, and an α value of around 0.33. The epitaxial buffer layers lay great foundation for the successful demonstration of epitaxial YBCO superconductor-coated conductors; however, the nucleation mechanism of the oxide buffers on metal surface is not fully understood as complex thermodynamic and kinetic stability are involved to form the ionic/nonionic interface. Reflection high-energy electron diffraction studies revealed that the formation of a c(2 × 2) two-dimensional superstructure on the

metal surface could promote the epitaxial oxide growth, which might be the possible mechanism (Cantoni et al., 2001).

Besides the successful demonstration of epitaxial YBCO superconducting thin films on buffered metal tapes, other functional oxides have also been obtained with epitaxial quality. Wee et al. deposited epitaxial Cu_2O thin film on Ni-W substrate with STO/CeO_2/YSZ/Y_2O_3 buffer layers, as shown in the schematic illustration in the inset of Figure 2B (Wee et al., 2015). The standard θ-2θ XRD scan in Figure 2B indicates the highly out-of-plane textured growth of all the layers. Figures 2C–2E present (111) pole figure, (002) ω-scans for both rolling (φ = 0°) and transverse (φ = 90°) directions, and (111) φ-scan of the Cu_2O thin film, respectively, all indicating the epitaxial quality of the film. Specifically, the full-width-half-maximum values of ω- and φ-scans can be determined as small as 2.4° and 4.9°, while 94% of cube texture was estimated from the clear 4-fold symmetry of the φ-scan, all indicating the excellent cube-on-cube epitaxy of Cu_2O thin film on STO/CeO_2/YSZ/Y_2O_3 buffered Ni-W substrate. The buffered metal foils serve as promising flexible substrates for the direct high-temperature growth of epitaxial oxide thin films, more and more flexible oxide films have been realized, including $BaTiO_3$ (BTO) (Shin et al., 2009), $Ce_{0.9}Zr_{0.1}O_{2-y}$ (CZO) (Queralto et al., 2015), $La_2Zr_2O_7$ (Mos et al., 2013), Pb(Zr, Ti)O_3 (PZT) (Shelton and Gibbons, 2011), $BiFeO_3$-$BiMnO_3$ (Xiong et al., 2014), etc.

Direct growth on flexible mica

Another promising candidate substrate for flexible oxide films is mica, because of its high melting point (1300°C), oxide-based crystal structure, cleavable layered structure (becomes flexible while being cleaved into ultrathin form), and ultrasmooth surface. The 2D layered structure of mica with dangling-bonds-free surface leads to the van der Waals (vdW) contact between the grown film on top and mica underneath, so-called vdW epitaxy (Bitla and Chu, 2017). Conventional epitaxy involves strong film/substrate interface interactions and chemical bonds orient across the interface, therefore certain lattice and thermal expansion matching is required, which restricts the universality of film/substrate combinations. On the other hand, weak film/substrate interaction is involved in vdW epitaxy, which mitigates lattice and thermal mismatch between the film and the underlying 2D substrate. Therefore, vdW epitaxy on mica largely extends the growth of epitaxial oxide thin films with mechanical flexibility.

Large amount of oxides with different crystal structures have been successfully demonstrated on mica with high epitaxial quality. For example, epitaxial ferroelectric PZT thin film has been grown on $SrRuO_3$ (SRO)/Co-Fe_2O_4 (CFO) double-buffered mica (Jiang et al., 2017). The θ-2θ XRD scan in Figure 3A indicates only PZT (*lll*) and SRO (*lll*) with mica (00*L*) diffraction peaks appear, and the φ-scans of PZT {002}, SRO {002}, CFO {004}, and mica {202} reflections in Figure 3B suggest the in-plane epitaxial relationship between the layers to be (111)SRO//(111)PZT//(001)mica and [1–10]SRO//[1–10]PZT//[010]mica. Furthermore, the reciprocal space mapping of PZT (002), SRO (002), and CFO (004) reflections in Figure 3C further confirms the epitaxial nature of the PZT ferroelectric film. Lastly, the cross-sectional TEM images of the PZT/SRO and SRO/CFO/mica interfaces along with the selected area diffraction patterns of PZT, SRO, and mica in Figure 3D indicate the clean interface, as well as the high epitaxial quality of each layer. The high-quality PZT film results in excellent ferroelectric property, as indicated by the representative local piezoresponse force microscopy (PFM) amplitude and phase hysteresis loops in Figure 3E, which presents 180° change in PFM phase and a clear butterfly loop. The flexible ferroelectric PZT film has also been tested for the mechanical strain effect, as illustrated in the inset of Figure 3F, the results in Figure 3F show that the local coercive fields of unbent state increase slowly under bending. Overall, the flexible PZT film on mica exhibits high epitaxial quality and excellent ferroelectricity, which can be tuned by mechanical strain. Besides, other oxides have also been demonstrated, including transparent conducting oxides Al-ZnO (AZO) and ITO (Bitla et al., 2016), magnetic CFO (Liu et al., 2017a, 2017b), $BaFe_{12}O_{19}$ (Ke et al., 2021) and Fe_3O_4 (Zheng et al., 2018), antiferroelectric $PbHfO_3$ (PHO) (Tsai et al., 2021) and $PbZrO_3$ (PZO) (Ko et al., 2021), wide bandgap semiconductor Ga_2O_3 (Tak et al., 2020), conducting SRO (Liu et al., 2018), ferroelectric Pr-doped $Ba_{0.85}Ca_{0.15}Ti_{0.9}Zr_{0.1}O_3$ (BCTZ:Pr) (Zheng et al., 2019a), $BiFeO_3$ (BFO) (Sun et al., 2020a, 2020b) and PZT (Jiang et al., 2017), colossal magnetoresistance $Pr_{0.5}Ca_{0.5}MnO_3$ (PCMO) (Yen et al., 2020), phase transition VO_2 (Li et al., 2016), etc.

Among all the oxide/mica heterostructures, it is interesting to note that the cubic (e.g. perovskite, spinel structures) oxides prefer [111] orientation growth, while hexagonal oxides are likely to grow along [001] direction. Both growth patterns result in quasihexagonal in-plane structure, which is in compatible with the hexagonally arrayed pattern of oxygen atoms in the basal plane [001] of mica. In principle, no lattice and crystal structure matching is required in vdW epitaxy as no chemical bonds formed between film and

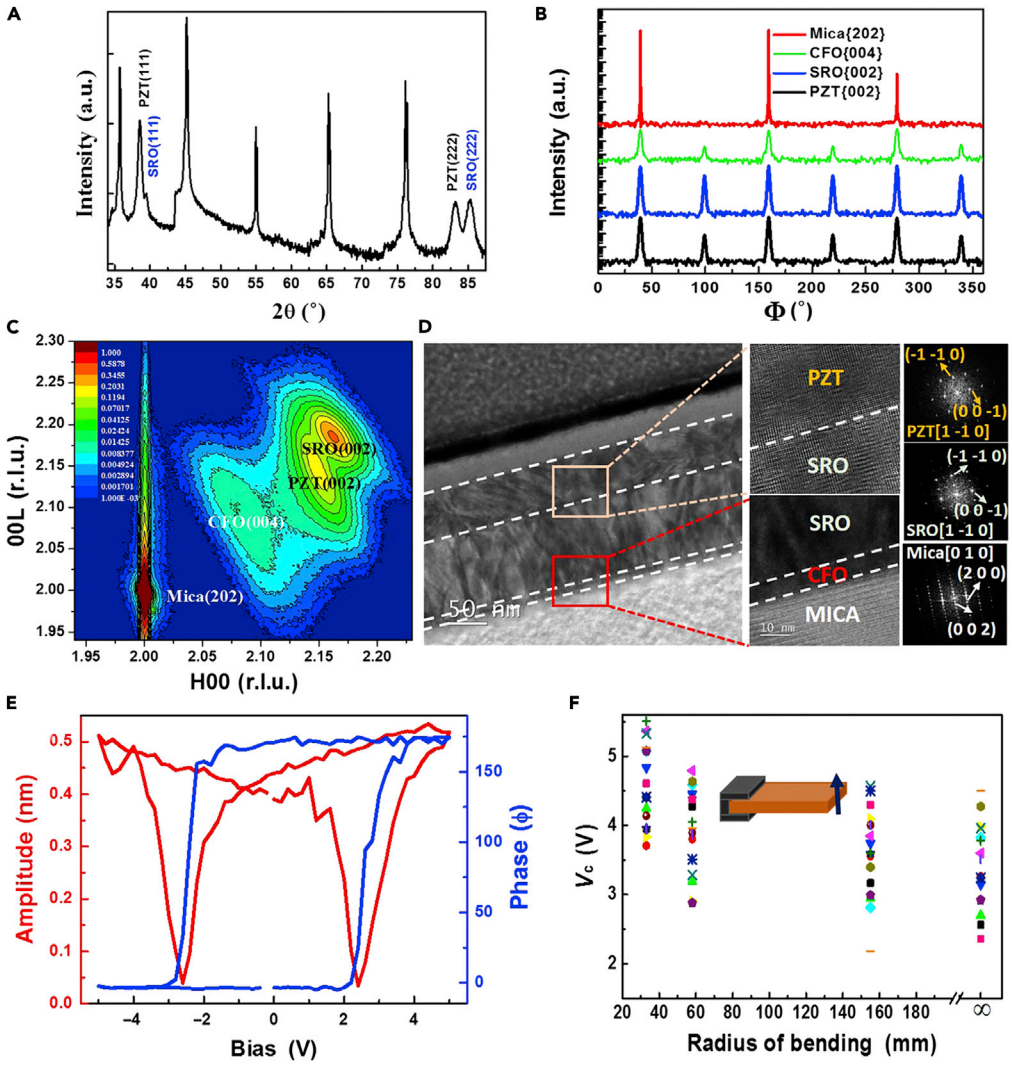

Figure 3. Direct growth of oxide thin films on flexible mica

(A) Standard θ-2θ XRD scan of the heterostructure; (B) φ-scans at PZT{002}, SRO{002}, CFO{004}, and mica{202} diffraction peaks; (C) The reciprocal space mapping of the heterostructure; (D) The cross-sectional TEM image showing the PZT/SRO and SRO/CFO/mica interfaces along with the selected area diffraction patterns of PZT, SRO, and mica; (E) Representative local PFM amplitude and phase hysteresis loops; (F) The local coercive voltage variation as a function of bending radius (Jiang et al., 2017). Reprinted with permission from the American Association for the Advancement of Science.

substrate; however, the grown films seem like following the preferred lattice extension on mica with the same crystal structure. Therefore, to understand the mechanism of the heteroepitaxy of oxides on mica, it is critical to investigate the oxides/mica heterointerface structure. Lu et al. applied atomic scale microscopy to explore the oxide/mica heterointerface using STO/mica as the model system (Lu et al., 2020). Figure 4A presents an STEM high angle angular dark field (HAADF) image of the STO/mica interface, recorded along mica [100] direction (or STO [110]). An interfacial layer of 0.86 nm was observed between the last K atom plane of the mica substrate and the first Sr-O_3 plane of the STO film, which can be further confirmed by the STEM angular bright field (ABF) image shown in Figure 4B. The interfacial structure indicates strong interaction between the (111) Sr-O_3 atomic plane of STO and the (001) $(SiAl)_2$-O_3 atomic plane of mica, because of the strong similarity of the oxygen network. This study indicates that the oxides/mica interfacial interaction plays an important role for the film growth. In addition, some reports show that perovskite films can be grown with other crystallographic orientations rather than [111], which suggests the growth condition is also a key point to determine the heteroepitaxial relationship in oxides/mica (Ye et al., 2022; Huang et al., 2018a, 2018b).

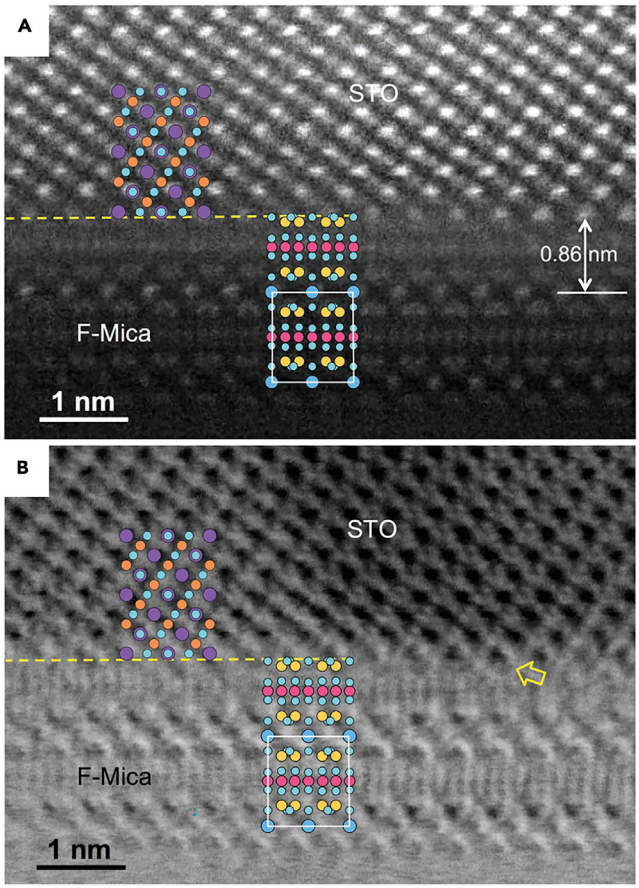

Figure 4. Microstructure of oxide/mica interface

(A) HAADF image and (B) ABF image of an STO/mica interface area, recorded along mica [100] direction (parallel to the [110] direction of STO). Corresponding projected structures of STO and mica are attached on both images, showing the termination of the STO film and the mica substrate at the interface (Lu et al., 2020). Reprinted with permission from John Wiley and Sons.

To further demonstrate more functionalities and flexible applications, oxide-based multilayer and composite thin films on mica have also been explored, such as multiferroic Fe_3O_4/$BiFeO_3$ bilayer (Zheng et al., 2019a, 2019b) and BFO-CFO composite system (Amrillah et al., 2017), exchange bias effect systems of Co/CoO (Ha et al., 2020a, 2020b) and $CoFe_2O_4$/CoO (Ha et al., 2020a, 2020b) bilayer and $La_{0.67}Sr_{0.33}MnO_3$ (LSMO)-NiO composite thin film (Huang et al., 2020a, 2020b, 2020c), as well as the recently developed $BaTiO_3$-Au (Liu et al., 2020a, 2020b) and $BaZrO_3$-Co (Liu et al., 2022a, 2022b) oxide-metal composite thin films. The oxides/mica heteroepitaxy provides a great platform to employ functional oxides in flexible electronics and spintronics, termed MICAtronics (Bitla and Chu, 2017). Recently, wafer-scale epitaxial oxide has been realized, which further suggests the promising device integration of oxides/mica for industry applications (Chen et al., 2021a, 2021b).

Lift-off and transfer of freestanding oxide thin films

To overcome the contradiction of the low melting point of the traditional flexible polymer substrates and the high-temperature processing for high-quality epitaxial oxide thin films, freestanding thin film is an ideal form as it can be transferred to any substrate. Lift-off process is involved to obtain freestanding thin films, which allows the separation of the film and substrate by either physical etching or chemical etching.

Physical etching method

Laser is the used resource for the physical etching, which etches the film/substrate interfacial area to separate the film and the substrate. The phonon energy of the laser should be in between the bandgap energy

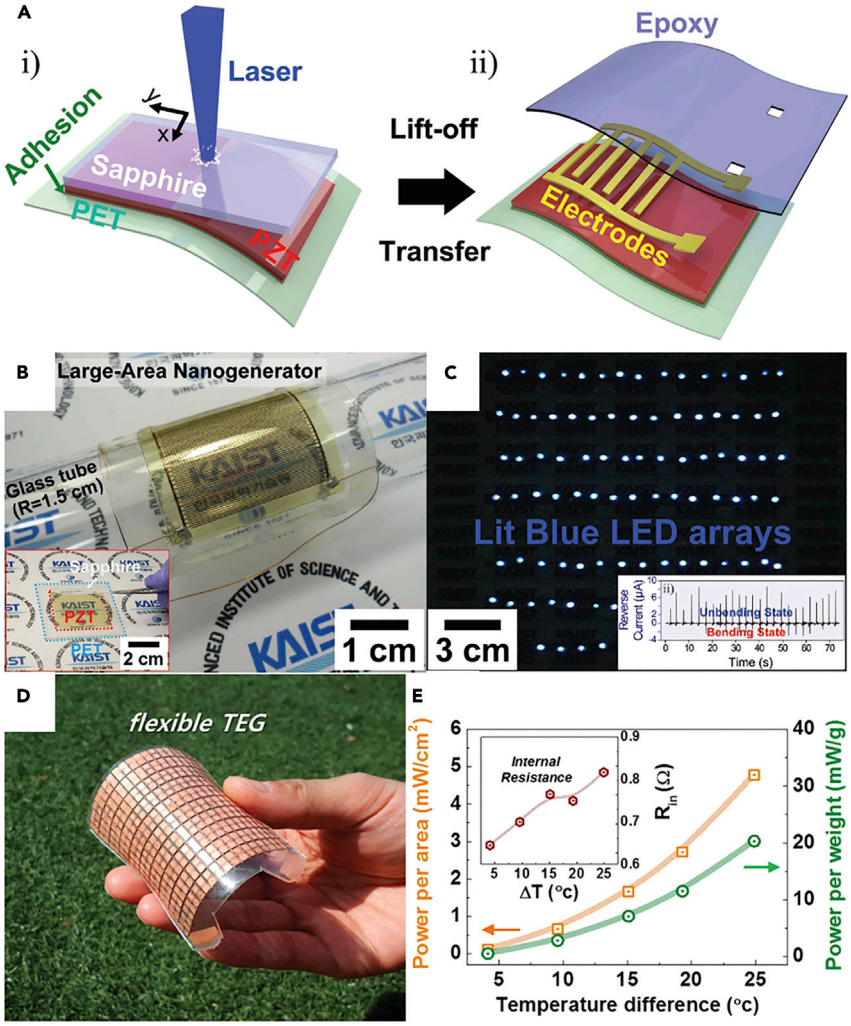

Figure 5. Flexible freestanding oxide thin films made by physical etching

(A) Schematic illustration of the fabrication process for the flexible large-scale PZT thin-film-based nanogenerator using the laser lift-off method; (B) Actual image of the real device. The inset shows a large-area PZT thin film transferred on PET substrate; (C) A snapshot showing the instantaneous lighting up of 105 blue LEDs in series when the flexible nanogenerator was unbent after slight bending by a human finger. The inset shows current signals measured from the device (Park et al., 2014). Reprinted with permission from John Wiley and Sons. (D) Actual photo of the freestanding f-TEG prepared using the laser lift-off process; (E) Output power per unit area and unit weight. The inset shows the change of internal resistance with respect to ΔT (Kim et al., 2016). Reprinted with permission from American Chemical Society.

levels of the film and the substrate. As the energy of the laser is lower than the energy level of the substrate, the incident laser on the backside of the substrate penetrates into the interfacial area and absorbed by the film, then the interfacial area starts to partial melt and dissociate to form the freestanding film.

Such method has been applied to obtain freestanding oxide thin films, which can be transferred on flexible polymer substrates for flexible device integration (Joe et al., 2017). For example, Park et al. fabricated flexible and large-area PZT thin film through laser etching technique, as shown in Figure 5A (Park et al., 2014). The PZT film was first deposited on rigid sapphire substrate at high temperature (~650°C), and then the film was detached from the substrate by the irradiation of a XeCl excimer laser at the backside of the substrate, followed by transferring to a PET substrate. Such flexible piezoelectric PZT film was then used as a large-scale (3.5 × 3.5 cm) energy harvester (nanogenerator) after the formation of an interdigitated electrode, as shown in Figure 5B is the actual device. The nanogenerator can produce output voltage of 250 V and output current of 8.8 μA, which could be used to light more than hundred commercial blue LEDs without any

rectifiers or charge circuits, as shown in Figure 5C. This method has also been adopted by Kim et al. to fabricate 4-inch-scale flexible thermoelectric generator (f-TEG, shown in Figure 5D), which presents excellent output power density of 4.78 mW/cm^2 at ΔT = 25 K (shown in Figure 5E) and the performance is robust even after 8000 bending cycles (Kim et al., 2016).

The laser lift-off method serves an effective approach for large-scale flexible oxide thin film fabrication and device integration (Jeong et al., 2017; Tsakalakos and Sands, 2000). However, certain substrate and laser should be selected to satisfy the high-quality film growth, as well as the energy states requirement of the film, substrate, and laser source. Furthermore, the laser irradiation process should be carefully controlled as it might damage the film with over-incident.

Chemical etching method

Corresponding to physical etching method, chemical etching has also been developed to realize freestanding oxide thin films for flexible applications. The basic idea is to use particular chemical solutions that can dissolve the substrate or sacrificial layer but inert to the film, then freestanding oxide film can be obtained by dissolving the substrate or sacrificial layer. Different oxides are soluble to certain chemicals with certain etching rate (Bridoux et al., 2012), which can be selected as the sacrificial layer or substrate.

Water-soluble $Sr_3Al_2O_6$ (SAO) sacrificial layer. Water-soluble material might be the most ideal candidate to be the sacrificial layer, since it is gentle to most oxides. $Sr_3Al_2O_6$ (SAO) is a water-soluble material constructed by cubic unit cells with the lattice parameter of a = 15.844 Å (matches well with four unit cells of $SrTiO_3$, a = 3.905 Å), which is perfect for epitaxial oxide thin film growth. Various oxide thin films with epitaxial quality have been successfully achieved, such as LSMO, STO, LSMO/STO superlattice (Lu et al., 2016), SRO (Le, ten Elshof and Koster, 2021), Fe_3O_4 (Hou et al., 2021), VO_2 (Han et al., 2021), YBCO (Chen et al., 2019), $PbTiO_3$ (PTO) (Han et al., 2020), $La_{0.7}Ca_{0.3}MnO_3$ (LCMO) (Park et al., 2020), BTO (Dong et al., 2019), etc. Furthermore, this method is applicable to achieve freestanding ultrathin BFO film down to the monolayer limit (Ji et al., 2019), as well as the recently developed LSMO:NiO nanocomposite thin film (Huang et al., 2022), all indicate the universality of this SAO sacrificial approach.

The procedure of the sacrificial layer method to obtain freestanding oxide thin films is simple; however, some particulars should be taken into account to attain clean and crackless freestanding films. Four different "etching and transfer" methods with the main difference of the support layer have been proposed and compared, which results in different quality of the transferred films (Zhang et al., 2021). Method I is to use sacrificial polymethyl-methacrylate (PMMA) as the support; however, the film is easy to break when detaching from the original substrate. In method II, PI tape (pressure sensitive adhesive tape) is employed as the support layer, which can prevent the transferred films from breaking, however it is difficult to release the films to other non-adhesive substrates. In method III, thermal release tape or silicone-coated PET has been used as the support as it can be removed by heating; however, voids, cracks, and some residues from the thermal release tape are inevitable after transfer. Lastly, in method IV, a two-layer structure support of PET frame/PMMA has been developed, which combines the advantages of method II and III, and results in clean and crackless freestanding films. Therefore, the appropriate support is critical for achieving large-scale high-quality freestanding oxide thin films. Other than that, the surface quality of the SAO sacrificial layer is also important, optimization has been done to obtain SAO layer with atomically smooth surface (Sun et al., 2020a, 2020b). In addition, low-cost facile chemical route has been employed to develop scalable water-soluble SAO films (Salles et al., 2021).

Other sacrificial layers. Although water-soluble SAO might be the most ideal sacrificial material, other materials have also been used as sacrificial layer to achieve high-quality freestanding oxide thin films. The "etching and transfer" process is the same as the SAO method, the only difference is that some certain chemicals are involved instead of water. The sacrificial layer can be a thin buffer layer, or sometimes the entire substrate can be etched to form the freestanding film. For example, Gan et al. deposited epitaxial SRO thin film on STO substrate, and then etched the STO substrate by using an acid solution of 50% HF: 70% HNO_3:H_2O = 1:1:1 (Gan et al., 1998; Paskiewicz et al., 2015). The etching rate for SRO and STO is found to be 1:9100 by this acid solution (Deneke et al., 2011), therefore the STO substrate is etched while leaving the SRO film nearly unaffected. MgO substrate was also etched by being immersed into 10% phosphoric acid aqueous solution at 40°C for several hours to obtain freestanding epitaxial BTO film grown on top (Nishikawa et al., 2021).

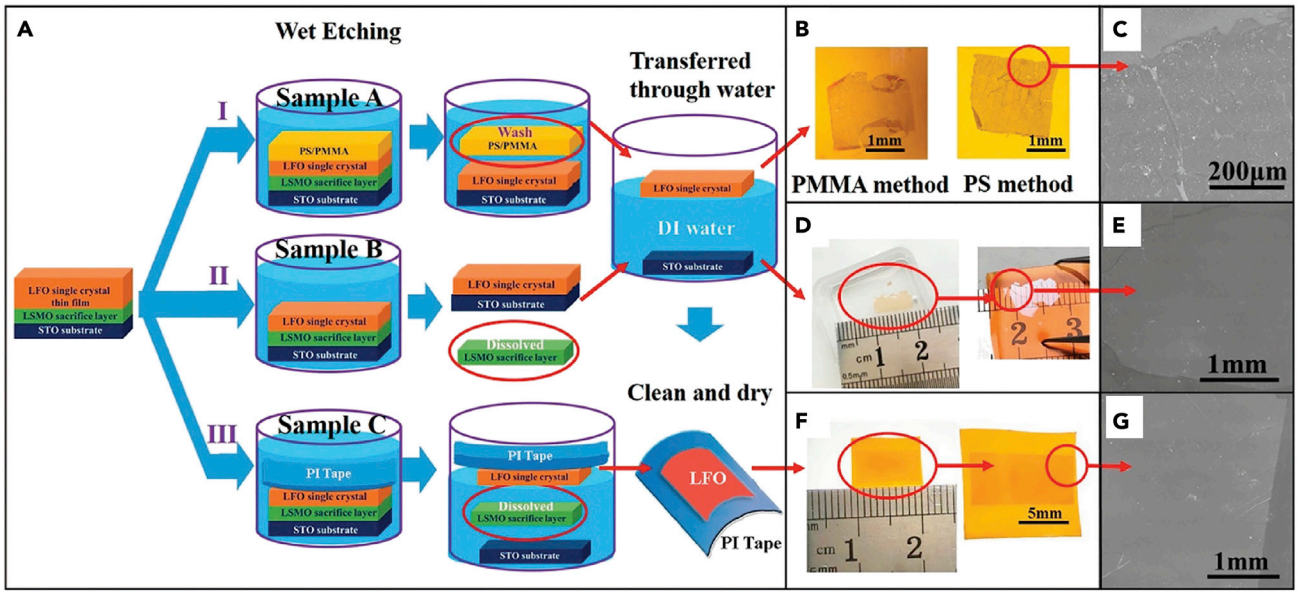

Figure 6. Flexible freestanding oxide thin films made by chemical etching

(A) Schematics of three different transfer methods to obtain flexible single-crystalline LFO films; (B), (D), (F) The optical photographs of the transferred films fabricated through Methods I, II, and III, respectively; (C), (E), (G) The corresponding SEM images, showing the microstructural features of the transferred films using different transfer methods (Shen et al., 2017). Reprinted with permission from John Wiley and Sons.

The substrate etching approach has some restrictions, for example, the selection of single-crystal substrate is limited and the substrate cannot be reused after etching. Furthermore, the relatively thick substrate resulting in long etching time, therefore a thin sacrificial layer is preferable. LSMO has been frequently used as sacrificial layer (Bakaul et al., 2017, 2020; Shen et al., 2017). For example, Shen et al. grew $LiFe_5O_8$ (LFO) thin film on STO substrate with ~30 nm LSMO buffer layer, and etchant of (400 mg KI + 10 mL HCl +500 mL H_2O) was used to etch the LSMO layer (Shen et al., 2017). Three methods with different support layers have been applied for the transfer process, as shown in Figure 6A, PMMA or polystyrene (PS) layer, no coating layer, and PI tape have been used for method I, II, and III, respectively. For method I, some cracks and random damages are observed in the freestanding film (shown in Figures 6B and 6C), which are induced by the residues and dispersed pieces from PMMA or PS during dissolving. Then, in method II, much smoother and cleaner freestanding film can be obtained (shown in Figures 6D and 6E); however, the film is usually torn into smaller pieces. Finally, in method III, the adhesive PI tape could coat the entire film without damage (shown in Figures 6F and 6G); however, it is difficult to detach the film from the tape. These methods with different supports result in the same film quality compared to the SAO approach as discussed above.

The LSMO sacrificial layer has also been used to fabricate ferroelectric PZT film for flexible memory application (Bakaul et al., 2017, 2020). In addition, other sacrificial materials have been used to obtain different freestanding oxide films, for example, MgO sacrificial layer is employed to achieve freestanding CFO by etching MgO using 10% $(NH_4)_2SO_4$ solution at 80°C (Zhang et al., 2017), and YBCO is used as the sacrificial layer to obtain freestanding LSMO and SRO films by etching YBCO using 0.6% hydrochloric acid (Chang et al., 2020).

Remote epitaxy method

Remote epitaxy is an emerging technique to obtain freestanding thin films with high quality, which can be mechanically exfoliated and transferred to flexible substrates (Kim et al., 2022). In such method, ultrathin 2D van der Waals materials are introduced as interlayer between the crystalline substrates and the oxide thin films grown on top. Kum et al. demonstrated that atomic potential fields can penetrate completely through bilayer graphene and partially through trilayer graphene, which suggests that the remote epitaxy could be realized with the graphene interlayer thinner than three monolayers (Kum et al., 2020). However, the exfoliation area yield of the sample is relatively low with one monolayer

graphene interlayer; therefore, bilayer graphene is the ideal thickness for graphene-based remote epitaxy to produce oxide thin films with high quality and high exfoliation yield. Ideally, this method could be utilized to fabricate freestanding single-crystalline oxide thin films with varying crystal structure and crystallographic orientations. For example, Ma et al. deposited various oxide thin films (ZnO, NiO, STO, and CFO) on different crystalline oxide substrate with MoS_2 as the interlayer (Ma et al., 2021). Other than that, epitaxial $BaTiO_{3-\delta}$ thin film on Ge (Dai et al., 2022) and yttrium iron garnet film on gadolinium gallium garnet (Leontsev et al., 2022) have been achieved by applying graphene as the interlayer. The remote epitaxy method has been employed more and more on fabricating freestanding epitaxy oxide thin films, which could be a critical approach toward both fundamental research and practical applications of epitaxial oxide thin films.

Overall, the "direct growth", "sacrificial layer and transfer", and "remote epitaxy" methods have been developed to achieve flexible oxide thin films with high epitaxial quality. For direct growth, metal foil and mica are the most used flexible substrates as they satisfy the high-temperature process of the epitaxial oxide films. The former requires tedious surface polishing process and a set of buffer layers are needed, while the latter needs to be cleaved to an ultrathin form to be flexible and the films are easy to be detached from the substrate due to the weak vdW bonding between them. Then, for the sacrificial layer and transfer method, different materials have been used as the sacrificial layer and the support is the key point to decide the quality of the transferred films. Lastly, the recently demonstrated remote epitaxy method is promising to develop freestanding oxide thin films with high epitaxial quality. The comparison of all the methods being used to achieve flexible oxide thin films is listed in Table 1, certain approach could be selected for the development of particular material.

FUNCTIONALITIES AND APPLICATIONS OF FLEXIBLE OXIDE THIN FILMS

Functionalities of flexible films

Up-to-date, various flexible oxide thin films have been demonstrated with different functionalities, such as ferroelectricity, magnetism, multiferroicity, superconductivity, transparent conductivity, etc. Two aspects are mainly considered for the functionalities of flexible oxides, one is the property robustness of the flexible films after tremendous bending cycles, the other is strain engineering of the flexible oxide films under certain bending condition. Strain is widely used to tailor the physical properties of oxides, which can be easily realized in flexible oxide films by bending the samples. For example, the magnetic properties (e.g. saturation magnetization and Curie temperature) in flexible SRO can be tuned through bending induced strain (Liu et al., 2018), and metal-insulator transition temperature and optical properties can be tuned in flexible VO_2 thin film by strain engineering (Chen et al., 2021a, 2021b).

Besides the conventional functionalities in oxides, some extraordinary physical phenomenon was also discovered. Dong et al. fabricated freestanding BTO thin film through SAO sacrificial layer and transfer method and used *in situ* SEM to study its mechanical property (Dong et al., 2019). Specifically, one nano-manipulator tip was used to hold the freestanding BTO film, and another nano-manipulator tip was used to bend it into different curvatures, as shown in Figure 7A. The bent film with 40° bending angle could be fully recovered in 10 s and such bending angle can be increased to as large as 80°, which indicates the super-elasticity of the freestanding BTO film. Considering the brittle nature of bulk BTO, the super-elasticity in freestanding BTO film is surprising. Two reasons have been proposed, the first is the low flaw density in epitaxial film, which avoids stress concentration and suppress the nucleation of crack in the interior of the sample. Another reason is the formation of a transition zone connecting *a* and *c* domains, which could largely eliminate the mismatch stress in the coexisting *a* and *c* nanodomains at high strain, avoiding the mechanical failure by the sharp domain switching. Such super-elasticity has also been found in freestanding Fe_3O_4 thin film, the flexibility with a bending radius as small as 7.18 μm and twist angle as large as 122° could be achieved, while no magnetic property degradation was observed under such large deformation. (An et al., 2020).

In addition, the flexible freestanding oxide thin film can approach the 2D limit, which might lead to exotic properties that do not exist in film/solid substrate form. For example, Ji et al. applied the SAO sacrificial layer method to obtain ultrathin BFO films down to 1 unit cell thick with high crystallinity. (Ji et al., 2019) Interestingly, the R-like as-grown film transferred to T-like freestanding film in the three-unit-cell sample, as shown in Figure 7B. Such phase or structure transition only occurs in the freestanding films thinner than four-unit-cell, as indicated by the c/a ratio and the offset of Fe ions from the centers of four

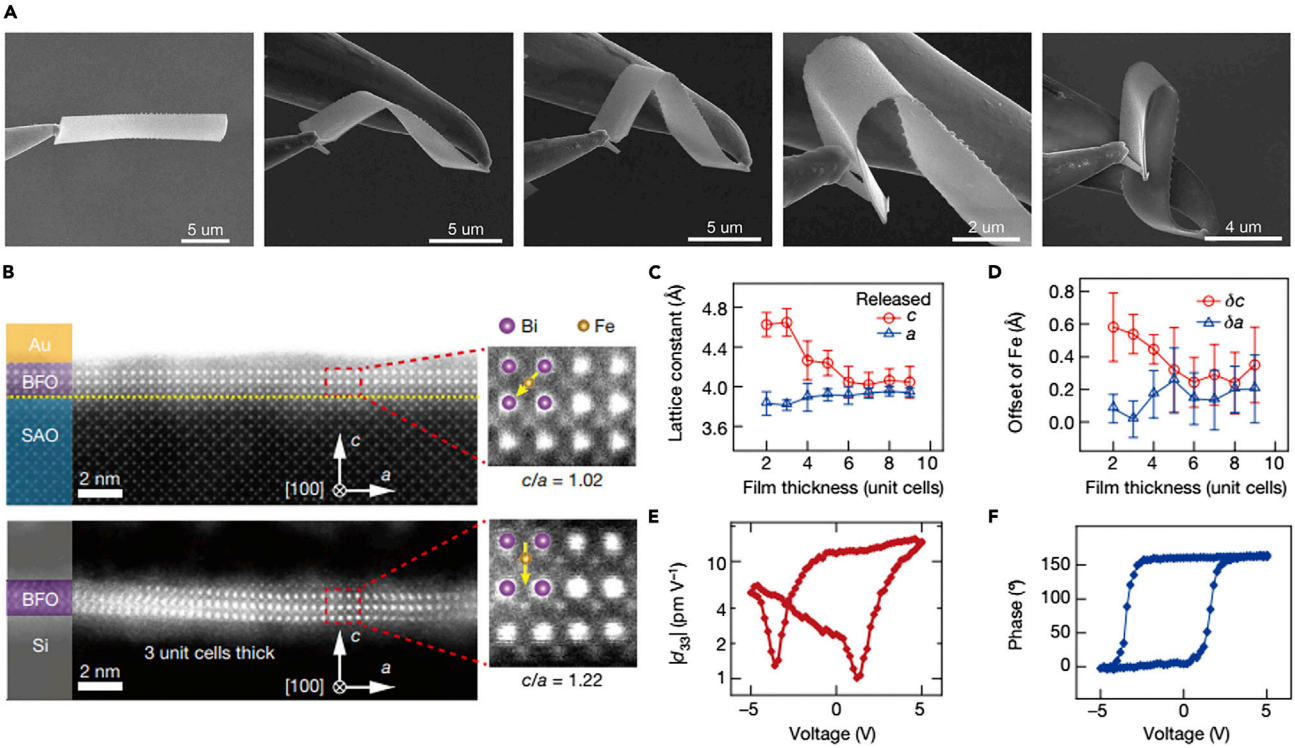

Figure 7. Extraordinary properties of the freestanding oxide thin films

(A) *In situ* SEM bending test of freestanding BTO nanobelts, series of SEM images with the bending process of a BTO nanobelt (Dong et al., 2019). Reprinted with permission from the American Association for the Advancement of Science.

(B) Cross-sectional HAADF images of a three-unit-cell BFO film before and after releasing; (C) The c/a ratio and (D) the offset of Fe ions from the centers of four neighboring Bi ions as a function of the thickness of freestanding BFO films. The error bars represent the fitting error of the lattice constants; (E) PFM amplitude-voltage butterfly loop and (F) phase-voltage hysteresis loop of a four-unit-cell freestanding BFO film on a conductive silicon substrate, showing that the polarization is switchable (Ji et al., 2019). Reprinted with permission from Spring Nature.

neighboring Bi ions in Figures 7C and 7D, respectively. The ultrathin BFO films thinner than four-unit cell obtain an abnormally large c/a ratio (up to 1.22) and polarization (140 μC cm^{-2}) along the out-of-plane direction. The PFM measurements shown in Figures 7E and 7F further confirm the excellent ferroelectricity and switchable polarization even in these ultrathin freestanding BFO films. The unexpected giant tetragonality and polarization in those ultrathin freestanding films was resulting from the stereochemical activity of a lone pair of bielectrons in R-phase BFO and displacement of Fe ions from the centrosymmetric position, as well as the surface electric field in the ultrathin films.

The exploration of novel physical properties in flexible freestanding oxide film is quite exciting, what makes it more interesting is the strain engineering on the films by mechanical deformation, which is effective for property modulation. Hong et al. developed $La_{0.7}Ca_{0.3}MnO_3$ (LCMO) membrane on flexible polymer supporter with strong adhesion, as shown in Figure 8A. (Hong et al., 2020) The strain state of the LCMO film can be controlled by clamping and stretching the polymer supporter, as the strain can be transferred from the polymer owing to the strong adhesion between them. Biaxial and uniaxial strain can be applied by stretching in two or one axis, which as shown in the electric potential mapping of the central vdP geometry in Figures 8B–8F, respectively. For biaxially strained LCMO films, increased ρ(300 K) and lower T_C of the FM-M/PM-I phase transition were obtained in higher strained films (Figure 8C), which is because of the reduction of the in-plane orbital overlap between Mn d orbitals and O p orbitals under tensile strain. Furthermore, an unexpected insulating phase appears at high biaxial strain states (>3%) at low temperatures, which can be quenched by magnetic fields with a large negative magnetoresistance, as shown in Figures 8D and 8E. Then, for the uniaxial strained films, a large resistance anisotropy could be obtained in the directions parallel (Figure 8G) and perpendicular (Figure 8H) to the uniaxial strain direction. From the results, nonmetallic temperature dependence was first observed in the parallel R-T curves (ε = 6 to 8%) and exist in the perpendicular

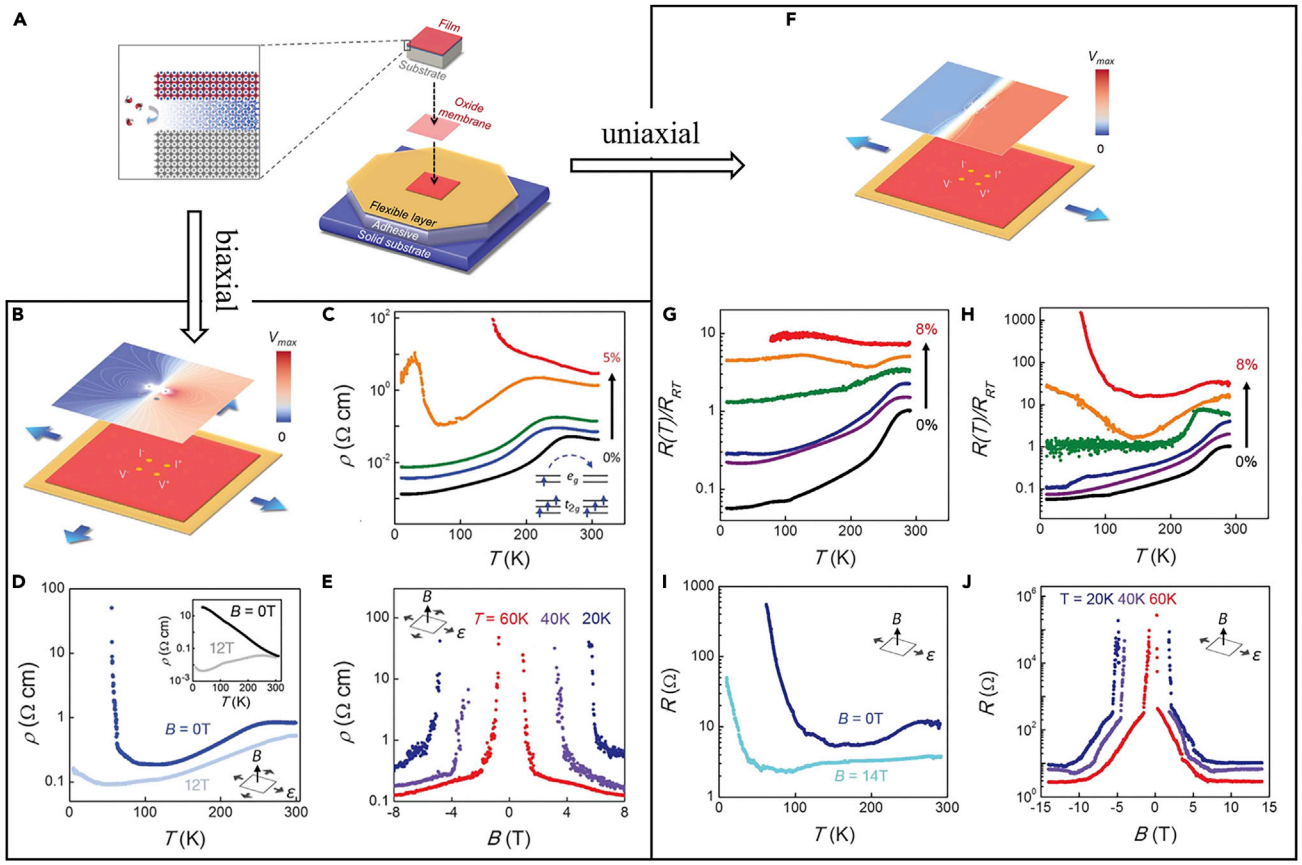

Figure 8. Strain engineering of freestanding oxide thin films

(A) Schematic platform for straining oxide membranes; (B) Electric potential mapping of the central vdP geometry in (B) biaxially and (F) uniaxial strained LCMO membranes; Resistivity-temperature (R-T) curves of 8-nm-thick LCMO membrane with (C) biaxially strain and (G) parallel and (H) perpendicular to the uniaxial strain as a function of strain. Inset of (C): Double exchange interaction between two Mn sites; R-T curves of (D) biaxially strained LCMO membrane (d = 4 nm, ε = 3.5%) and (I) uniaxially strained LCMO membrane (vdP resistance perpendicular to the strain ε = 8%) under perpendicular magnetic field. Inset of (D): Same measurements on LCMO film grown on STO substrate; Magnetoresistance (MR) of (E) biaxially and (J) uniaxially strained LCMO membranes at different temperatures (Hong et al., 2020). Reprinted with permission from the American Association for the Advancement of Science.

direction at larger strains (ε = 7 to 8%). Such insulating states can be largely suppressed with external magnetic field, and large magnetoresistance was achieved, as shown in Figures 8I and 8J. This work demonstrates that the physical properties of the flexible oxide films can be effectively modulated via strain engineering, which provides a great platform for property regulation of flexible oxide films.

As is seen, different flexible oxide thin films have been successfully demonstrated with epitaxial quality, which present all functionalities that exist in solid state form. The physical properties can be further tuned by strain engineering, which can be realized by stretching the flexible samples. In another side, strain gradient or nonuniform lattice distortion can be induced by bending the flexible oxide films, which results in tunable flexoelectricity to modulate the photoconductance in flexible BFO thin film (Guo et al., 2020). In addition, the flexible or freestanding films can induce novel and unexpected properties that cannot be found in their bulk counterpart or unbent state. Therefore, the flexible oxide thin films provide great platform to discover new functionalities.

Applications of flexible films

The final goal of the development of the flexible oxide thin films is to employ them in the integration of flexible devices. Thanks to the large evolution of the various methods developed to fabricate flexible oxide thin films with high epitaxial quality, it is very promising to use them in high-performance flexible devices. As-so-far, some oxide-based flexible electronics has been proposed, such as flexible energy storage (Tsai et al.,

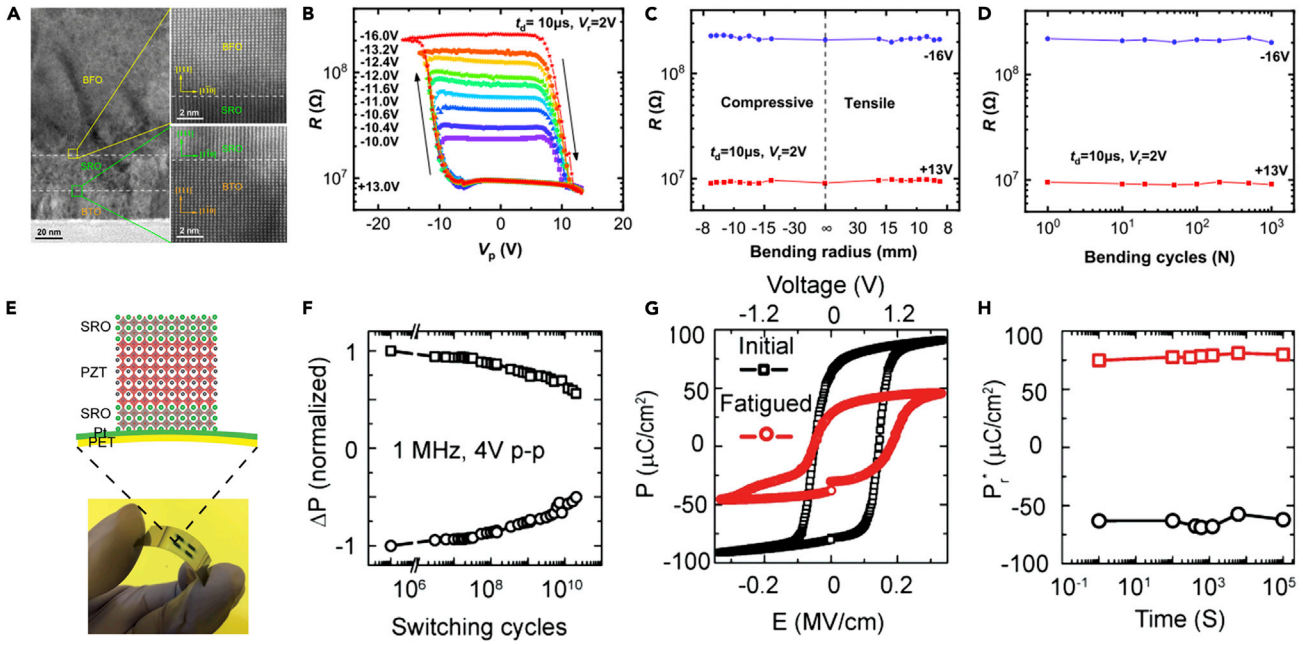

Figure 9. Flexible ferroelectric memory

(A) Cross-sectional TEM image of the BFO/SRO/BTO/mica heterostructure; (B) Resistances as a function of V_p with t_d = 10 μs; Resistance switchings between the ON and OFF states at different (C) bending radii and (D) bending cycles under the bending radius of 8 mm at the compressive condition (Sun et al., 2020a, 2020b). Reprinted with permission from American Chemical Society.

(E) Photograph of the flexed SRO/PZT/SRO memory device on PET; (F) Fatigue test of the device on a bent (10 mm radius of curvature) substrate; (G) P-E test before and after 3 × 10^{10} switching cycles; (H) Time dependence of the memory state showing unchanged remnant polarization for 10^5 s (Bakaul et al., 2017). Reprinted with permission from John Wiley and Sons.

2021; Ko et al., 2021), flexible ferroelectric memory (Sun et al., 2020a, 2020b; Le et al., 2019; Yang et al., 2019; Kim et al., 2014), flexible acoustic nanosensors (Lee et al., 2014), flexible nanogenerator (Park et al., 2014), etc.

Flexible ferroelectric memory

Ferroelectricity-induced resistance switching has been widely demonstrated in BFO thin films on rigid substrates, which exhibits the potential in building artificial synaptic devices (Boyn et al., 2017). In such device, the resistance of the films could be gradually tuned via the ferroelectric domain switching, which avoids the unstable filament forming/rupture process in conventional memristors. Sun et al. deposited ferroelectric BFO film on SRO/BTO buffered mica, which follows [111] growth orientation and presents high epitaxial quality, as shown in Figure 9A (Sun et al., 2020a, 2020b). To test the memristor behaviors of this flexible BFO-based heterostructure, SRO buffer layer was used as the bottom electrode and Au was deposited on top as the top electrode. With the pulse duration t_d = 10 μs, the memristor was set to the lowest resistance state (ON state) by +13 V (the ferroelectric polarization points to the SRO bottom electrode), or the highest resistance state (OFF state) by −16 V (the ferroelectric polarization points to the Au top electrode), the resistance state can be tuned to intermediate states by applying different voltage pulse $-V_p^{max-}$, as shown in Figure 9B. Then, to test the robustness of the flexible memristor, the resistance switchings between ON and OFF states were explored under different bending conditions, as shown in Figures 9C and 9D are at different bending radii and bending cycles, respectively. The results show that the performance of the memristor is almost identical under all tested bending radii and after 10^3 bending cycles, which indicates the high flexibility and stability of such BFO-based memristor.

Bakaul et al. used layer transfer technique to develop SRO/PZT/SRO flexible memory device, as illustrated in Figure 9E (Bakaul et al., 2017). Then, fatigue, retention, and bending cycling measurements have been tested to probe the reliability of the flexible memory device on a bent (10 mm radius of curvature) substrate, as shown in Figures 9F, 9G, and 9H, respectively. The results show that the ferroelectricity retains 50% of the initial remnant polarization after 3 × 10^{10} times switching. Furthermore, no degradation of remnant polarization was observed after 10^5 s, which indicates the device might satisfy the industry-standard of 10 years'

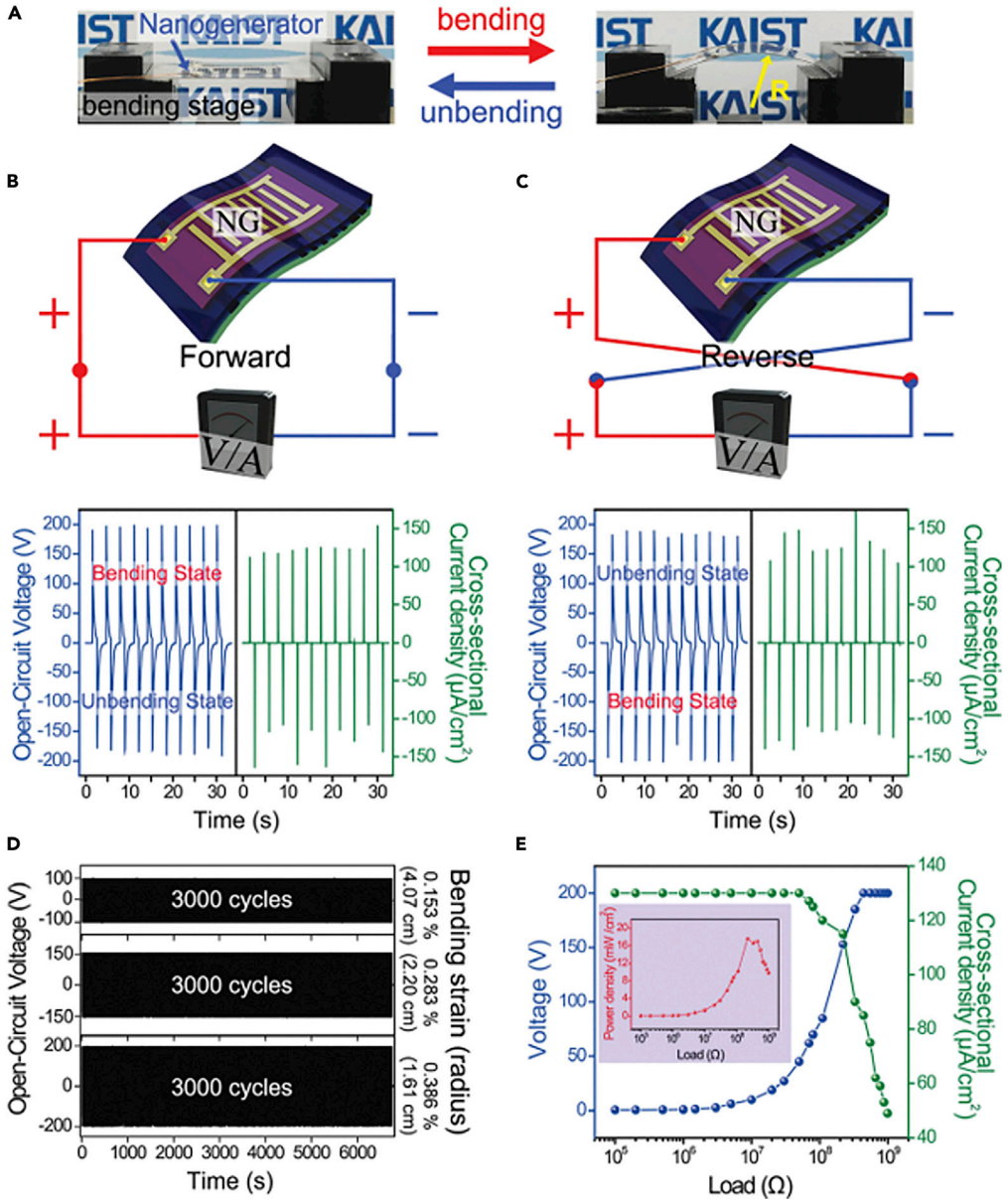

Figure 10. Flexible energy devices

(A) Photographs of PZT thin film NG captured at unbending and bending states; The open-circuit voltage and cross-sectional current density measured from PZT thin film NG in the (B) forward and (C) reverse connections; (D) Strain dependence and mechanical stability of output voltage generated from PZT thin film NG; (E) The measured output voltage and cross-sectional current density under different load resistance varying from 2 kΩ to 1 GΩ. The inset shows the relationship between the output power and external resistance (Park et al., 2014). Reprinted with permission from John Wiley and Sons.

data retention. Such flexible memory device has also been realized in AZO/NiO/AZO (Le et al., 2019) and Au/Bi($Fe_{0.93}Mn_{0.05}Ti_{0.02}$)$O_3$/Pt (Yang et al., 2019) heterostructures, and flexible crossbar-structured 32 × 32 resistive random access memory arrays based on Ni/NiO_x/Ti/Pt heterostructure has also been developed (Kim et al., 2014).

Flexible energy devices

Nanogenerator (NG) converts mechanical energy into electricity, which can utilize the piezoelectric materials to harvest energy from human movements. The external mechanical force induces the center offset

between the positive and negative charges in piezoelectric materials, which results in a potential difference. Park et al. fabricated flexible and large-area PZT thin film NG using laser lift-off method, as introduced in the above section on the discussion of physical etching method to make the flexible oxide films (Park et al., 2014). Figure 10A presents the real image of the flexible NG under bending and unbending states, and the output voltage and current signal were measured to explore the energy conversion efficiency of the device. A linear bending motor with a strain of ~0.386% at a straining rate of ~2.32%·s^{-1} was applied to induce the mechanical deformation of the flexible NG. When the device was in forward connection state, the open-circuit voltage and the short-circuit current exceed 200 V and 1.5 μA, respectively, which generates a cross-sectional current density of 150 μA cm^{-2}), as shown in Figure 10B. When the device was in reverse connection state, the measured signals were opposite, which confirms the piezoelectric effect induced electricity in this flexible PZT thin film NG, as shown in Figure 10C. The performance of the device under different bending states was also compared in Figure 10D. The bending states of 0.153%, 0.283%, and 0.386% result in output voltage of ~100 V (top), ~160 V (center), and ~200 V (bottom), respectively. Furthermore, the device was connected to the external load resistance ranging from 2 kΩ to 1 GΩ, and the voltage and current signals were compared in Figure 10E. From the results, the voltage gradually increases with the increasing resistance until being saturated at a certain high resistance, while the current is consistent initially and starts to decreases with higher resistance. The instantaneous power density can be calculated to be 17.5 mW cm^{-2} at a resistance of 200 MΩ, as shown in the inset of Figure 10E. The flexible energy devices have also been demonstrated in flexible antiferroelectric oxides, as they exhibit high energy-storage density and efficiency, such as flexible $PbHfO_3$ (PHO) (Tsai et al., 2021) and $PbZrO_3$ (PZO) (Ko et al., 2021) thin films.

Other flexible devices

The flexible device has the advantage of mechanical flexibility, which could induce functionalities that cannot be realized in rigid device, especially the mechanical deformation-related properties. For example, PZT inorganic-based piezoelectric acoustic nanosensor (iPANS) has been developed to work as biomimetic artificial hair cell to mimic the functions of the original human hair cells, and the flexible PZT thin film on flexible plastic was obtained through laser lift-off method (Lee et al., 2014). This iPANS exhibits highly sensitivity and could effectively convert sound energy into piezoelectric signals in the audible frequency range of living noise (40 dB SPL). In addition, the transparent conductive oxides can be used as electrode for flexible devices. Jia et al. developed highly flexible, robust, stable, and high-efficient perovskite solar cells using ITO on mica as the flexible electrode and support (Jia et al., 2019), which indicates the flexible oxide thin films can work as one component in some flexible devices.

Flexible oxide-based thin film transistors (TFTs) are highly demanded for next-generation displays, radio-frequency identification (RFID) tags, as well as integrated circuits (Jeon et al., 2022; He et al., 2018). No epitaxial quality is needed for the oxide thin films in TFTs, therefore low-temperature processing methods have been applied for the flexible devices, such as atomic layer deposition (Cho et al., 2019; Park et al., 2015) and solution-based processing (e.g. spin coating, spray coating, flexographic printing, and inkjet printing) (Leppäniemi et al., 2015; Song et al., 2010). Further work is needed to improve the device performance through material property optimization and device structure design. The low-temperature-processed oxide thin films have also been achieved as the electrodes for flexible perovskite solar cells (Zhang et al., 2020a, 2020b; Girtan and Negulescu, 2022), which extends the application field of the flexible oxides.

CONCLUSIONS AND FUTURE PERSPECTIVES

In conclusion, different fabrication methods have been developed to obtain flexible functional oxide thin films with high quality, the normal functionalities and novel physical phenomenon have been reviewed, and the oxide-based flexible devices have been introduced. Generally, the flexible oxide thin films can be obtained by either "direct growth on flexible substrates" or "freestanding film transfer" approaches. The former employs the thin metal foils or inorganic cleavable mica as the flexible substrates, while the latter involves freestanding thin films. For the films on flexible metal foils, a set of buffer layers are always required to ensure the quality of the oxide films grown on top, which is widely used for the fabrication of high-temperature superconductor-coated conductors. Mica takes the advantages of both mechanically flexible and high melting temperature, could serve as a perfect substrate to achieve high-quality flexible oxide thin films. Various oxides have been epitaxially grown on mica with robust physical properties. However, as

Table 1. Comparison of the different methods to achieve flexible oxide thin films

Methods		Advantages	Drawbacks
Direct Growth	Metal Foil	Direct one-step growth; Suitable for large-scale processing.	Tedious surface polishing required; A set of buffers needed.
	Mica		Needs to be cleaved to an ultrathin form to be flexible; Films are easy to be detached from mica; Insulating mica is not ideal for some electronic devices.
Lift-off and Transfer	Physical Etching	Suitable for large-scale processing, simple process.	Films might be damaged with over-incident;
	Chemical Etching	Simple process, various sacrificial layers could be selected to achieve different oxide thin films.	Cracks might be generated in the films; Some chemicals might be harmful to the oxide films; Certain supports are needed to obtain high-quality films.
Remote Epitaxy		Suitable to grow oxide thin films with varying crystal structure and crystallographic orientations.	Large-scale processing is difficult; Careful thickness control of the 2D material interlayer is needed.

an insulating material, mica might not be ideal for some electronic devices. For the latter "freestanding film transfer" method, physical or chemical etching has been applied to obtain the freestanding oxide films and then transfer onto any flexible wafers. There are two potential issues, one is that the etching process might deteriorate the target oxide films, the other is that certain support is needed to avoid the cracks, folds, and other flaws in the transferred films.

With the large development of the fabrication methods, different functionalities or properties have been demonstrated in different flexible oxide films. Compared to the same film on rigid substrates, the flexible films show some unique properties (e.g. super-elasticity) and strain engineering can be easily applied by bending process to tune the physical properties. Finally, flexible devices have been designed to fully utilize the flexible oxide films, such as flexible memory, flexible energy harvesting device, flexible sensor, etc.

Although extensive progress has been achieved in the field from the aspects of fabrication methods, functionalities, and applications, there is still tremendous space and further efforts are needed for this promising direction. (i) For the aspect of fabrication, direct growth is the most ideal approach, therefore it is highly demanded to develop low-temperature epitaxy approach; the recently reported spin coating epitaxy provides opportunity (Kelso et al., 2019; Liu et al., 2020a, 2020b). Furthermore, for the freestanding films, cracks or voids usually appear during the etching and transfer processes, therefore such technique should be further optimized, such as the etching solution and the support materials. Lastly, remote epitaxy technology could be further improved along with the development of large-scale 2D materials, which will provide an excellent platform to produce large-scale freestanding epitaxial oxide thin films. (ii) For the aspect of functionalities, most of the current demonstrated flexible oxide films are based on single-phase materials, to realize more functionalities or multifunctionality, flexible oxide-based composite thin films are desirable, such as 0–3 type nanoparticle-in-matrix structure (Huang et al., 2018a, 2018b, 2021a, 2021b, 2021c, 2021d, 2021e; Qi et al., 2018), 1–3 type nanopillar-in-matrix structure (Huang et al., 2021a, 2021b, 2021c, 2021d, 2021e; Fan et al., 2017; Huang et al., 2021a, 2021a, 2021b, 2021b, 2021b, 2021c, 2021c, 2021c, 2021d, 2021d, 2021d, 2021e, 2021e, 2021e; Zhang et al., 2020a, 2020b), as well as 2-2 type multilayers (Huang et al., 2020a, 2020a, 2020b, 2020b, 2020b, 2020b, 2020c, 2020c, 2021a, 2021b, 2021c, 2021d, 2021e; Huang et al., 2020a, 2020b; Sun et al., 2018). In addition, the freestanding or flexible oxide films provide a perfect platform for flexoelectricity; some unique physical properties might be discovered (Cai et al., 2022; Chen et al., 2015). Finally, freestanding oxide thin films are ideal for some fundamental exploration, such as how the surface effect and bending condition affect the atomic construction, as well as the local physical properties. (iii) For the aspect of devices, currently most of the fabricated flexible devices based on oxide films are in single-device form; device arrays are highly demanded for practical application in industrial level (Kim et al., 2014; Jeon et al., 2022). In another hand, oxides are ceramics with high brittleness and low malleability, therefore the life of the oxide-based flexible devices might be fatal issue. (iv) Some pioneer theoretical work has been done on the close relationship between physical properties and mechanical bending of the flexible oxides, (Zheng et al., 2008; Li et al., 2014)

which needs to be realized in experimental studies. Lastly, flexible oxides with novel nanostructures could be developed to achieve exotic physical phenomenon, such as nanoribbons or wavy thin films. (Feng et al., 2011; Chen et al., 2014).

ACKNOWLEDGMENTS

This work was supported by the National Natural Science Foundation of China (Grants No. 11972382, No. 12132020), Guangdong Basic and Applied Basic Research Foundation (2019A1515111029), and Shenzhen Science and Technology Program (JCYJ20210324133610028).

AUTHOR CONTRIBUTIONS

J.H. conceived the idea and initiated the project. J.H. and W.C. conducted the literature review. J.H. and W.C. wrote the manuscript. J.H. prepared the figures. All authors read and provided feedback on the manuscript. J.H. and W.C. guided the entire work.

DECLARATION OF INTERESTS

The authors declare no competing interests.

REFERENCES

Acharya, S.K., Nallagatla, R.V., Togibasa, O., Lee, B.W., Liu, C., Jung, C.U., Park, B.H., Park, J.Y., Cho, Y., Kim, D.W., et al. (2016). Epitaxial brownmillerite oxide thin films for reliable switching memory. ACS Appl. Mater. Interfaces *8*, 7902–7911. https://doi.org/10.1021/acsami.6b00647.

Amrillah, T., Bitla, Y., Shin, K., Yang, T., Hsieh, Y.H., Chiou, Y.Y., Liu, H.J., Do, T.H., Su, D., Chen, Y.C., et al. (2017). Flexible multiferroic bulk heterojunction with giant magnetoelectric coupling via van der Waals epitaxy. ACS Nano *11*, 6122–6130. https://doi.org/10.1021/acsnano.7b02102.

An, F., Qu, K., Zhong, G., Dong, Y., Ming, W., Zi, M., Liu, Z., Wang, Y., Qi, B., Ding, Z., et al. (2020). Highly flexible and twistable freestanding single crystalline magnetite film with robust magnetism. Adv. Funct. Mater. *30*, 2003495. https://doi.org/10.1002/adfm.202003495.

Bakaul, S.R., Serrao, C.R., Lee, O., Lu, Z., Yadav, A., Carraro, C., Maboudian, R., Ramesh, R., and Salahuddin, S. (2017). High speed epitaxial perovskite memory on flexible substrates. Adv. Mater. *29*, 1605699. https://doi.org/10.1002/adma.201605699.

Bakaul, S.R., Kim, J., Hong, S., Cherukara, M.J., Zhou, T., Stan, L., Serrao, C.R., Salahuddin, S., Petford-Long, A.K., Fong, D.D., and Holt, M.V. (2020). Ferroelectric domain wall motion in freestanding single-crystal complex oxide thin film. Adv. Mater. *32*, 1907036. https://doi.org/10.1002/adma.201907036.

Bao, Z., and Chen, X. (2016). Flexible and stretchable devices. Adv. Mater. *28*, 4177–4179. https://doi.org/10.1002/adma.201601422.

Bitla, Y., Chen, C., Lee, H.C., Do, T.H., Ma, C.H., Qui, L.V., Huang, C.W., Wu, W.W., Chang, L., Chiu, P.W., and Chu, Y.H. (2016). Oxide heteroepitaxy for flexible optoelectronics. ACS Appl. Mater. Interfaces *8*, 32401–32407. https://doi.org/10.1021/acsami.6b10631.

Bitla, Y., and Chu, Y.H. (2017). MICAtronics: a new platform for flexible X-tronics. FlatChem *3*, 26–42. https://doi.org/10.1016/j.flatc.2017.06.003.

Boyn, S., Grollier, J., Lecerf, G., Xu, B., Locatelli, N., Fusil, S., Girod, S., Carrétéro, C., Garcia, K., Xavier, S., et al. (2017). Learning through ferroelectric domain dynamics in solid-state synapses. Nat. Commun. *8*, 14736. https://doi.org/10.1038/ncomms14736.

Bridoux, G., Barzola-Quiquia, J., Bern, F., Böhlmann, W., Vrejoiu, I., Ziese, M., and Esquinazi, P. (2012). An alternative route towards micro- and nano-patterning of oxide films. Nanotechnology *23*, 085302. https://doi.org/10.1088/0957-4484/23/8/085302.

Cai, S., Lun, Y., Ji, D., Han, L., Guo, C., Zang, Y., Gao, S., Wei, Y., Gu, M., Zhang, C., et al. (2022). Giant polarization and abnormal flexural deformation in bent freestanding perovskite oxides. Preprint at arXiv. https://doi.org/10.48550/arXiv.2009.03177.

Cantoni, C., Christen, D.K., Feenstra, R., Goyal, A., Ownby, G.W., Zehner, D.M., and Norton, D.P. (2001). Reflection high-energy electron diffraction studies of epitaxial oxide seed-layer growth on rolling-assisted biaxially textured substrate Ni (001): the role of surface structure and chemistry. Appl. Phys. Lett. *79*, 3077–3079. https://doi.org/10.1063/1.1407857.

Chang, Y.W., Wu, P.C., Yi, J.B., Liu, Y.C., Chou, Y., Chou, Y.C., and Yang, J.C. (2020). A fast route towards freestanding single crystalline oxide thin films by using $YBa_2Cu_3O_{7-x}$ as a sacrificial layer. Nanoscale Res. Lett. *15*, 172. https://doi.org/10.1186/s11671-020-03402-0.

Chen, H.W., Li, C.I., Ma, C.H., Chu, Y.H., and Liu, H.L. (2021a). Strain engineering of optical properties in transparent VO_2/muscovite heterostructures. Phys. Chem. Chem. Phys. *23*, 8908–8915. https://doi.org/10.1039/d1cp00642h.

Chen, W.A., Gluck, G.S., and Li, Z. (2015). Utilizing mechanical loads and flexoelectricity to induce and control complicated evolution of domain patterns in ferroelectric nanofilms. Tech. Hand Up. Extrem. Surg. *19*, 108–109. https://doi.org/10.1016/j.jmps.2015.04.003.

Chen, W.J., Zheng, Y., Xiong, W.M., Feng, X., Wang, B., and Wang, Y. (2014). Effect of mechanical loads on stability of nanodomains in ferroelectric ultrathin films: towards flexible erasing of the non-volatile memories. Sci. Rep. *4*, 5339. https://doi.org/10.1038/srep05339.

Chen, Y.C., Tu, Y.H., Chen, L.W., Lai, Y.H., Tsai, M.F., Lin, Y.X., Lai, H.C., Chiang, C.Y., Liu, H.J., Pan, H.C., et al. (2021b). Fabrication of large-scale high-mobility flexible transparent zinc oxide single crystal wafers. ACS Appl. Mater. Interfaces *13*, 18991–18998. https://doi.org/10.1021/acsami.1c01782.

Chen, Z., Wang, B.Y., Goodge, B.H., Lu, D., Hong, S.S., Li, D., Kourkoutis, L.F., Hikita, Y., and Hwang, H.Y. (2019). Freestanding crystalline $YBa_2Cu_3O_{7-x}$ heterostructure membranes. Phys. Rev. Materials *3*, 060801. (R). https://doi.org/10.1103/PhysRevMaterials.3.060801.

Cho, M.H., Seol, H., Song, A., Choi, S., Song, Y., Yun, P.S., Chung, K.B., Bae, J.U., Park, K.S., and Jeong, J.K. (2019). Comparative study on performance of IGZO transistors with sputtered and atomic layer deposited channel layer. IEEE Trans. Electron. Dev. *66*, 1783–1788. https://doi.org/10.1109/TED.2019.2899586.

Dai, L., Zhao, J., Li, J., Chen, B., Zhai, S., Xue, Z., Di, Z., Feng, B., Sun, Y., Luo, Y., et al. (2022). Highly heterogeneous epitaxy of flexoelectric $BaTiO_{3-\delta}$ membrane on Ge. Nat. Commun. *13*, 2990. https://doi.org/10.1038/s41467-022-30724-7.

Dawber, M., Rabe, K.M., and Scott, J.F. (2005). Physics of thin-film ferroelectric oxides. Rev. Mod. Phys. *77*, 1083–1130. https://doi.org/10.1103/RevModPhys.77.1083.

Deneke, C., Wild, E., Boldyreva, K., Baunack, S., Cendula, P., Mönch, I., Simon, M., Malachias, A., Dörr, K., and Schmidt, O.G. (2011). Rolled-up tubes and cantilevers by releasing $SrRuO_3$-$Pr_{0.7}Ca_{0.3}MnO_3$ nanomembranes. Nanoscale Res. Lett. *6*, 621. https://doi.org/10.1186/1556-276X-6-621.

Dong, G., Li, S., Yao, M., Zhou, Z., Zhang, Y.Q., Han, X., Luo, Z., Yao, J., Peng, B., Hu, Z., et al. (2019). Super-elastic ferroelectric single-crystal membranewith continuous electric dipole

rotation. Science *366*, 475–479. https://doi.org/10.1126/science.aay7221.

Fabbri, F., Annino, C., Boffa, V., Celentano, G., Ciontea, L., Gambardella, U., Grimaldi, G., Mancini, A., and Petrisor, T. (2000). Properties of biaxially oriented Y_2O_3 based buffer layers deposited on cube textured non-magnetic Ni-V substrates for YBCO coated conductors. Phys. C Supercond. *341–348*, 2503–2504. https://doi.org/10.1016/S0921-4534(00)01295-8.

Fan, M., Zhang, B., Wang, H., Jian, J., Sun, X., Huang, J., Li, L., Zhang, X., Wang, H., et al. (2017). Self-organized epitaxial vertically aligned nanocomposites with long-range ordering enabled by substrate nanotemplating. Adv. Mater. *29*, 1606861. https://doi.org/10.1002/adma.201606861.

Feng, X., Yang, B.D., Liu, Y., Wang, Y., Dagdeviren, C., Liu, Z., Carlson, A., Li, J., Huang, Y., and Rogers, J.A. (2011). Stretchable ferroelectric nanoribbons with wavy configurations on elastomeric substrates. ACS Nano *5*, 3326–3332. https://doi.org/10.1021/nn200477q.

Foltyn, S.R., Civale, L., Macmanus-Driscoll, J.L., Jia, Q.X., Maiorov, B., Wang, H., and Maley, M. (2007). Materials science challenges for high-temperature superconducting wire. Nat. Mater. *6*, 631–642. https://doi.org/10.1038/nmat1989.

Gan, Q., Rao, R.A., Eom, C.B., Garrett, J.L., and Lee, M. (1998). Direct measurement of strain effects on magnetic and electrical properties of epitaxial thin films. Appl. Phys. Lett. *72*, 978–980. https://doi.org/10.1063/1.120603.

Gao, W., Emaminejad, S., Nyein, H.Y.Y., Challa, S., Chen, K., Peck, A., Fahad, H.M., Ota, H., Shiraki, H., Kiriya, D., et al. (2016). Fully integrated wearable sensor arrays for multiplexed in situ perspiration analysis. Nature *529*, 509–514. https://doi.org/10.1038/nature16521.

Girtan, M., and Negulescu, B. (2022). A review on oxide/metal/oxide thin films on flexible substrates as electrodes for organic and perovskite solar cells. Opt. Mater. X *13*, 100122. https://doi.org/10.1016/j.omx.2021.100122.

Goyal, A., Norton, D., Christen, D., Specht, E., Paranthaman, M., Kroeger, D., Budai, J., He, Q., List, F., Feenstra, R., et al. (1996a). Epitaxial superconductors on rolling-assisted biaxially-textured substrates (RABiTS): a route towards high critical current density wire. Appl. Supercond. *4*, 403–427. https://doi.org/10.1016/S0964-1807(97)00029-X.

Goyal, A., Norton, D.P., Budai, J.D., Paranthaman, M., Specht, E.D., Kroeger, D.M., Christen, D.K., He, Q., Saffian, B., List, F.A., et al. (1996b). High critical current density superconducting tapes by epitaxial deposition of $YBa_2Cu_3O_x$ thick films on biaxially textured metals. Appl. Phys. Lett. *69*, 1795–1797. https://doi.org/10.1063/1.117489.

Guo, C.F., and Ding, L. (2021). Integration of soft electronics and biotissues. Innovation *2*, 100074. https://doi.org/10.1016/j.xinn.2020.100074.

Guo, R., You, L., Lin, W., Abdelsamie, A., Shu, X., Zhou, G., Chen, S., Liu, L., Yan, X., Wang, J., and Chen, J. (2020). Continuously controllable photoconductance in freestanding $BiFeO_3$ by the macroscopic flexoelectric effect. Nat. Commun. *11*, 2571. https://doi.org/10.1038/s41467-020-16465-5.

Ha, T.D., Yen, M., Lai, Y.H., Kuo, C.Y., Chen, C.T., Tanaka, A., Tsai, L.Z., Zhao, Y.F., Duan, C.G., Lee, S.F., et al. (2020a). Mechanically tunable exchange coupling of Co/CoO bilayers on flexible muscovite substrates. Nanoscale *12*, 3284–3291. https://doi.org/10.1039/c9nr08810e.

Ha, T.D., Chen, J.W., Yen, M., Lai, Y.H., Wang, B.Y., Chin, Y.Y., Wu, W.B., Lin, H.J., Juang, J.Y., and Chu, Y.H. (2020b). Dynamical strain-driven phase separation in flexible $CoFe_2O_4$/CoO exchange coupling system. ACS Appl. Mater. Interfaces *12*, 46874–46882. https://doi.org/10.1021/acsami.0c11475.

Han, K., Wu, L., Cao, Y., Wang, H., Ye, C., Huang, K., Motapothula, M., Xing, H., Li, X., Qi, D.C., et al. (2021). Enhanced metal-insulator transition in freestanding VO_2 down to 5 nm thickness. ACS Appl. Mater. Interfaces *13*, 16688–16693. https://doi.org/10.1021/acsami.1c01581.

Han, L., Fang, Y., Zhao, Y., Zang, Y., Gu, Z., Nie, Y., and Pan, X. (2020). Giant uniaxial strain ferroelectric domain tuning in freestanding $PbTiO_3$ films. Adv. Mater. Interfaces *7*, 1901604. https://doi.org/10.1002/admi.201901604.

He, Y., Wang, X., Gao, Y., Hou, Y., and Wan, Q. (2018). Oxide-based thin film transistors for flexible electronics. J. Semicond. *39*, 011005. https://doi.org/10.1088/1674-4926/39/1/011005.

Hong, S.S., Gu, M., Verma, M., Harbola, V., Wang, B.Y., Lu, D., Vailionis, A., Hikita, Y., Pentcheva, R., Rondinelli, J.M., and Hwang, H.Y. (2020). Extreme tensile strain states in $La_{0.7}Ca_{0.3}MnO_3$ membranes. Science *368*, 71–76. https://doi.org/10.1126/science.aax9753.

Hou, W., Yao, M., Qiu, R., Wang, Z., Zhou, Z., Shi, K., Pan, J., Liu, M., and Hu, J. (2021). Epitaxial lift-off of flexible single-crystal magnetite thin films with tunable magnetic performances by mechanical deformation. J. Alloys Compd. *887*, 161470. https://doi.org/10.1016/j.jallcom.2021.161470.

Huang, J., Jin, T., Misra, S., Wang, H., Qi, Z., Dai, Y., Sun, X., Li, L., Okkema, J., Chen, H., et al. (2018a). Tailorable optical response of Au-$LiNbO_3$ hybrid metamaterial thin films for optical waveguide applications. Adv. Opt. Mater. *6*, 1800510. https://doi.org/10.1002/adom.201800510.

Huang, J., Wang, H., Sun, X., Zhang, X., and Wang, H. (2018b). Multifunctional $La_{0.67}Sr_{0.33}MnO_3$ (LSMO) thin films integrated on mica substrates toward flexible spintronics and electronics. ACS Appl. Mater. Interfaces *10*, 42698–42705. https://doi.org/10.1021/acsami.8b16626.

Huang, J., Wang, H., Wang, X., Gao, X., Liu, J., and Wang, H. (2020a). Exchange bias in a $La_{0.67}Sr_{0.33}MnO_3$/NiO heterointerface integrated on a flexible mica substrate. ACS Appl. Mater. Interfaces *12*, 39920–39925. https://doi.org/10.1021/acsami.0c12935.

Huang, J., Zhang, D., Qi, Z., Zhang, B., and Wang, H. (2021a). Hybrid Ag-$LiNbO_3$ nanocomposite thin films with tailorable optical properties. Nanoscale Adv. *3*, 1121–1126. https://doi.org/10.1039/d0na00975j.

Huang, J., Phuah, X.L., McClintock, L.M., Padmanabhan, P., Vikrant, K., Wang, H., Zhang, D., Wang, H., Lu, P., Gao, X., et al. (2021b). Core-shell metallic alloy nanopillars-in-dielectric hybrid metamaterials with magneto-plasmonic coupling. Mater. Today *51*, 39–47. https://doi.org/10.1016/j.mattod.2021.10.024.

Huang, J., Wang, H., Qi, Z., Lu, P., Zhang, D., Zhang, B., He, Z., and Wang, H. (2021c). Multifunctional metal-oxide nanocomposite thin film with plasmonic Au nanopillars embedded in magnetic $La_{0.67}Sr_{0.33}MnO_3$ matrix. Nano Lett. *21*, 1032–1039. https://doi.org/10.1021/acs.nanolett.0c04213.

Huang, J., Zhang, D., Liu, J., Dou, H., and Wang, H. (2021d). Double exchange bias modulation under horizontal and perpendicular field directions by 3D nanocomposite designs. ACS Appl. Mater. Interfaces *13*, 50141–50148. https://doi.org/10.1021/acsami.1c14699.

Huang, J., Zhang, D., and Wang, H. (2020b). Epitaxial TiN/MgO multilayers with ultrathin TiN and MgO layers as hyperbolic metamaterials in visible region. Materials Today Physics *16*, 100316. https://doi.org/10.1016/j.mtphys.2020.100316.

Huang, J., Wang, X., Li, D., Jin, T., Lu, P., Zhang, D., Lin, P., Chen, H., Narayan, J., Zhang, X., and Wang, H. (2020c). 3D hybrid plasmonic framework with Au nanopillars embedded in nitride multilayers integrated on Si. Adv. Mater. Interfaces *7*, 2000493. https://doi.org/10.1002/admi.202000493.

Huang, J., Li, W., Yang, H., and MacManus-Driscoll, J.L. (2021e). Tailoring physical functionalities of complex oxides by vertically aligned nanocomposite thin-film design. MRS Bull. *46*, 159–167. https://doi.org/10.1557/s43577-021-00028-0.

Huang, J., MacManus-Driscoll, J.L., and Wang, H. (2017). New epitaxy paradigm in epitaxial self-assembled oxide vertically aligned nanocomposite thin films. J. Mater. Res. *32*, 4054–4066. https://doi.org/10.1557/jmr.2017.281.

Huang, J., and Wang, H. (2017). Effective magnetic pinning schemes for enhanced superconducting property in high temperature superconductor $YBa_2Cu_3O_{7-x}$: a review. Supercond. Sci. Technol. *30*, 114004. https://doi.org/10.1088/1361-6668/aa8d32.

Huang, J., Zhang, D., Liu, J., and Wang, H. (2022). Freestanding $La_{0.7}Sr_{0.3}MnO_3$:NiO vertically aligned nanocomposite thin films for flexible perpendicular interfacial exchange coupling. Materials Research Letters *10*, 287–294. https://doi.org/10.1080/21663831.2022.2041502.

Jeon, Y., Lee, D., and Yoo, H. (2022). Recent advances in metal-oxide thin-film transistors: flexible/stretchable devices, integrated circuits, biosensors, and neuromorphic applications. Coatings *12*, 204. https://doi.org/10.3390/coatings12020204.

Jeong, C.K., Cho, S.B., Han, J.H., Park, D.Y., Yang, S., Park, K.I., Ryu, J., Sohn, H., Chung, Y.C., and Lee, K.J. (2017). Flexible highly-effective energy harvester via crystallographic and computational

control of nanointerfacial morphotropic piezoelectric thin film. Nano Res. *10*, 437–455. https://doi.org/10.1007/s12274-016-1304-6.

Jeong, Y.S., Park, J.H., and Lee, S.Y. (1998). Epitaxial growth of YBCO on Hastelloy with YSZ buffer layer by laser ablation. Thin Solid Films *318*, 262–264. https://doi.org/10.1016/S0040-6090(97)01186-3.

Ji, D., Cai, S., Paudel, T.R., Sun, H., Zhang, C., Han, L., Wei, Y., Zang, Y., Gu, M., Zhang, Y., et al. (2019). Freestanding crystalline oxide perovskites down to the monolayer limit. Nature *570*, 87–90. https://doi.org/10.1038/s41586-019-1255-7.

Jia, C., Zhao, X., Lai, Y.H., Zhao, J., Wang, P.C., Liou, D.S., Wang, P., Liu, Z., Zhang, W., Chen, W., et al. (2019). Highly flexible, robust, stable and high efficiency perovskite solar cells enabled by van der Waals epitaxy on mica substrate. Nano Energy *60*, 476–484. https://doi.org/10.1016/j.nanoen.2019.03.053.

Jiang, J., Bitla, Y., Huang, C.W., Do, T.H., Liu, H.J., Hsieh, Y.H., Ma, C.H., Jang, C.Y., Lai, Y.H., Chiu, P.W., et al. (2017). Flexible ferroelectric element based on van der Waals heteroepitaxy. Sci. Adv. *3*, e1700121. https://doi.org/10.1126/sciadv.1700121.

Joe, D.J., Kim, S., Park, J.H., Park, D.Y., Lee, H.E., Im, T.H., Choi, I., Ruoff, R.S., and Lee, K.J. (2017). Laser-material interactions for flexible applications. Adv. Mater. *29*, 1606586. https://doi.org/10.1002/adma.201606586.

Kacedon, D.B., Rao, R.A., and Eom, C.B. (1997). Magnetoresistance of epitaxial thin films of ferromagnetic metallic oxide $SrRuO_3$ with different domain structures. Appl. Phys. Lett. *71*, 1724–1726. https://doi.org/10.1063/1.120016.

Ke, W.E., Shao, P.W., Kuo, C.Y., Song, H., Huang, R., Yagi, N., Kimura, T., Bitla, Y., Chang, C.F., and Chu, Y.H. (2021). Barium hexaferrite/muscovite heteroepitaxy with mechanically robust perpendicular magnetic anisotropy. npj Flex. Electron. *5*, 33. https://doi.org/10.1038/s41528-021-00130-y.

Kelso, M.V., Mahenderkar, N.K., Chen, Q., Tubbesing, J.Z., and Switzer, J.A. (2019). Spin coating epitaxial films. Science *364*, 166–169. https://doi.org/10.1126/science.aaw6184.

Kim, H., Chang, C.S., Lee, S., Jiang, J., Jeong, J., Park, M., Meng, Y., Ji, J., Kwon, Y., Sun, X., et al. (2022). Remote epitaxy. Nat. Rev. Methods Primers *2*, 40. https://doi.org/10.1038/s43586-022-00122-w.

Kim, S., Son, J.H., Lee, S.H., You, B.K., Park, K.I., Lee, H.K., Byun, M., and Lee, K.J. (2014). Flexible crossbar-structured resistive memory arrays on plastic substrates via inorganic-based laser lift-off. Adv. Mater. *26*, 7480–7487. https://doi.org/10.1002/adma.201402472.

Kim, S.J., Lee, H.E., Choi, H., Kim, Y., We, J.H., Shin, J.S., Lee, K.J., and Cho, B.J. (2016). High-performance flexible thermoelectric power generator using laser multiscanning lift-off process. ACS Nano *10*, 10851–10857. https://doi.org/10.1021/acsnano.6b05004.

Ko, D.L., Hsin, T., Lai, Y.H., Ho, S.Z., Zheng, Y., Huang, R., Pan, H., Chen, Y.C., and Chu, Y.H. (2021). High-stability transparent flexible energy storage based on $PbZrO_3$/muscovite heterostructure. Nano Energy *87*, 106149. https://doi.org/10.1016/j.nanoen.2021.106149.

Kum, H.S., Lee, H., Kim, S., Lindemann, S., Kong, W., Qiao, K., Chen, P., Irwin, J., Lee, J.H., Xie, S., et al. (2020). Heterogeneous integration of singlecrystalline complex-oxide membranes. Nature *578*, 75–81.

Le, P.T.P., ten Elshof, J.E., and Koster, G. (2021). Epitaxial lift-off of freestanding (011) and (111) $SrRuO_3$ thin films using a water sacrificial layer. Sci. Rep. *11*, 12435. https://doi.org/10.1038/s41598-021-91848-2.

Le, V.Q., Do, T.H., Retamal, J.R.D., Shao, P.W., Lai, Y.H., Wu, W.W., He, J.H., Chueh, Y.L., and Chu, Y.H. (2019). Van der Waals heteroepitaxial AZO/NiO/AZO/muscovite (ANA/muscovite) transparent flexible memristor. Nano Energy *56*, 322–329. https://doi.org/10.1016/j.nanoen.2018.10.042.

Lee, H.S., Chung, J., Hwang, G.T., Jeong, C.K., Jung, Y., Kwak, J.H., Kang, H., Byun, M., Kim, W.D., Hur, S., et al. (2014). Flexible inorganic piezoelectric acoustic nanosensors for biomimetic artificial hair cells. Adv. Funct. Mater. *24*, 6914–6921. https://doi.org/10.1002/adfm.201402270.

Leontsev, S., Shah, P., Kum, H., McChesney, J., Rodolakis, F., van Veenendaal, M., Velez, M., Rao, R., Haskel, D., Kim, J., et al. (2022). Functional properties of Yttrium Iron Garnett thin films on graphene-coated $Gd_3Ga_5O_{12}$ for remote epitaxial transfer. J. Magn. Magn Mater. *556*, 169440. https://doi.org/10.1016/j.jmmm.2022.169440.

Leppäniemi, J., Huttunen, O.H., Majumdar, H., and Alastalo, A. (2015). Flexography-printed In_2O_3 semiconductor layers for high-mobility thin-film transistors on flexible plastic substrate. Adv. Mater. *27*, 7168–7175. https://doi.org/10.1002/adma.201502569.

Li, C.I., Lin, J.C., Liu, H.J., Chu, M.W., Chen, H.W., Ma, C.H., Tsai, C.Y., Huang, H.W., Lin, H.J., Liu, H.L., et al. (2016). van der Waal epitaxy of flexible and transparent VO_2 film on muscovite. Chem. Mater. *28*, 3914–3919. https://doi.org/10.1021/acs.chemmater.6b01180.

Li, H., Hu, S., Zhang, J., Zhou, J., Ran, H., Tang, Y., Chen, J., and Wang, Y. (2014). Ab initio study on mechanical-bending-induced ferroelectric phase transition in ultrathin perovskite nanobelts. Acupunct. Med. *32*, 472–477. https://doi.org/10.1016/j.actamat.2014.05.054.

List, F.A., Goyal, A., Paranthaman, M., Norton, D., Specht, E., Lee, D., and Kroeger, D. (1998). High J_c YBCO films on biaxially textured Ni with oxide bufferc layers deposited using electron beam evaporation and sputtering. Phys. C Supercond. *302*, 87–92. https://doi.org/10.1016/S0921-4534(98)00154-3.

Liu, C., An, F., Gharavi, P.S.M., Lu, Q., Zha, J., Chen, C., Wang, L., Zhan, X., Xu, Z., Zhang, Y., et al. (2020a). Large-scale multiferroic complex oxide epitaxy with magnetically switched polarization enabled by solution processing. Natl. Sci. Rev. *7*, 84–91. https://doi.org/10.1093/nsr/nwz143.

Liu, H.J., Wang, C.K., Su, D., Amrillah, T., Hsieh, Y.H., Wu, K.H., Chen, Y.C., Juang, J.Y., Eng, L.M., Jen, S.U., and Chu, Y.H. (2017b). Flexible heteroepitaxy of $CoFe_2O_4$/muscovite bimorph with large magnetostriction. ACS Appl. Mater. Interfaces *9*, 7297–7304. https://doi.org/10.1021/acsami.6b16485.

Liu, J., Feng, Y., Tang, R., Zhao, R., Gao, J., Shi, D., and Yang, H. (2018). Mechanically tunable magnetic properties of flexible $SrRuO_3$ epitaxial thin films on mica substrates. Adv. Electron. Mater. *4*, 1700522. https://doi.org/10.1002/aelm.201700522.

Liu, J., Wang, X., Gao, X., Wang, H., Jian, J., Huang, J., Sun, X., Qi, Z., Misra, S., He, Z., and Wang, H. (2020b). Multifunctional self-assembled $BaTiO_3$-Au nanocomposite thin films on flexible mica substrates with tunable optical properties. Appl. Mater. Today *21*, 100856. https://doi.org/10.1016/j.apmt.2020.100856.

Liu, J., Wang, X., Gao, X., Wang, H., Zhang, B., Zhang, D., Kalaswad, M., Huang, J., and Wang, H. (2022a). Integration of self-assembled $BaZrO_3$-Co vertically aligned nanocomposites on mica substrates toward flexible spintronics. Cryst. Growth Des. *22*, 718–725. https://doi.org/10.1021/acs.cgd.1c01227.

Liu, M., Ren, S.P., Zhang, R.Y., Xue, Z.Y., Ma, C.R., Yin, M.L., Xu, X., Bao, S.Y., and Chen, C.L. (2015). Gas sensing properties of epitaxial $LaBaCo_2O_{5-5+\delta}$ thin Films. Sci. Rep. *5*, 10784. https://doi.org/10.1038/srep10784.

Liu, Y., He, K., Chen, G., Leow, W.R., and Chen, X. (2017a). Nature-inspired structural materials for flexible electronic devices. Chem. Rev. *117*, 12893–12941. https://doi.org/10.1021/acs.chemrev.7b00291.

Liu, Z., Yin, Z., Jiang, Y., and Zheng, Q. (2022b). Dielectric interface passivation of polyelectrolyte-gated organic field-effect transistors for ultrasensitive low-voltage pressure sensors in wearable applications. Materials Today Electronics *1*, 100001. https://doi.org/10.1016/j.mtelec.2022.100001.

Lorenz, M., Ramachandra Rao, M.S., Venkatesan, T., Fortunato, E., Barquinha, P., Branquinho, R., Salgueiro, D., Martins, R., Carlos, E., Liu, A., et al. (2016). The 2016 oxide electronic materials and oxide interfaces roadmap. J. Phys. D Appl. Phys. *49*, 433001. https://doi.org/10.1088/0022-3727/49/43/433001.

Lu, D., Baek, D.J., Hong, S.S., Kourkoutis, L.F., Hikita, Y., and Hwang, H.Y. (2016). Synthesis of freestanding single-crystal perovskite films and heterostructures by etching of sacrificial water-soluble layers. Nat. Mater. *15*, 1255–1260. https://doi.org/10.1038/NMAT4749.

Lu, L., Dai, Y., Du, H., Liu, M., Wu, J., Zhang, Y., Liang, Z., Raza, S., Wang, D., and Jia, C. (2020). Atomic scale understanding of the epitaxy of perovskite oxides on flexible mica substrate. Adv. Mater. Interfaces *7*, 1901265. https://doi.org/10.1002/admi.201901265.

Ma, B., Li, M., Fisher, B.L., Koritala, R.E., and Balachandran, U. (2002). Epitaxial growth of YBCO films on metallic substrates buffered with yttria-stabilized zirconia. AIP Conf. Proc. *614*, 573. https://doi.org/10.1063/1.1472588.

Ma, C.H., Lu, L.S., Song, H., Chen, J.W., Wu, P.C., Wu, C.L., Huang, R., Chang, W.H., and Chu, Y.H. (2021). Remote growth of oxide heteroepitaxy through MoS_2. Apl. Mater. *9*, 051115. https://doi.org/10.1063/5.0045639.

MacManus-Driscoll, J.L. (2010). Self-assembled heteroepitaxial oxide nanocomposite thin film structures: designing interface-induced functionality in electronic materials. Adv. Funct. Mater. *20*, 2035–2045. https://doi.org/10.1002/adfm.201000373.

Matias, V., and Hammond, R.H. (2012). YBCO superconductor wire based on IBAD-textured templates and RCE of YBCO: process economics. Phys. Procedia *36*, 1440–1444. https://doi.org/10.1016/j.phpro.2012.06.239.

Mos, R.B., Petrisor, T., Gabor, M., Mancini, A., Rufoloni, A., Celentano, G., Falqui, A., Genovese, A., Ruffilli, R., Ciontea, L., and Petrisor, T. (2013). Epitaxial growth and characterization of $La_2Zr_2O_7$ multilayers on biaxially textured NiW substrate by chemical solution deposition under highly reducing conditions. Thin Solid Films *531*, 491–498. https://doi.org/10.1016/j.tsf.2013.01.099.

Nishikawa, H., Umatani, S., Mizuyama, T., Hiraoka, A., and Mikami, K. (2021). Giant wrinkles on the surface of epitaxial $BaTiO_3$ thin films with drastic shrinkage during transfer from a MgO(100) single-crystal substrate to a flexible polyethylene terephthalate sheet. Sensors *21*, 7326. https://doi.org/10.3390/s21217326.

Norton, D.P., Park, C., Prouteau, C., Christen, D., Chisholm, M., Budai, J., Pennycook, S., Goyal, A., Sun, E., Lee, D., et al. (1998). Epitaxial $YBa_2Cu_3O_7$ films on rolled-textured metals for high-temperature superconducting applications. Mater. Sci. Eng., B *56*, 86–94. https://doi.org/10.1016/S0921-5107(98)00230-X.

Park, J., Shin, J.H., Song, K., Kim, Y.J., Jang, H.B., Lee, H., Sim, H.S., and Yang, C.H. (2020). Non-Ohmic conduction in exfoliated $La_{0.7}Ca_{0.3}MnO_3$ thin films. Appl. Phys. Lett. *116*, 022401. https://doi.org/10.1063/1.5127355.

Park, K.I., Son, J.H., Hwang, G.T., Jeong, C.K., Ryu, J., Koo, M., Choi, I., Lee, S.H., Byun, M., Wang, Z.L., and Lee, K.J. (2014). Highly-efficient, flexible piezoelectric PZT thin film nanogenerator on plastic substrates. Adv. Mater. *26*, 2514–2520. https://doi.org/10.1002/adma.201305659.

Park, M.J., Yun, D.J., Ryu, M.K., Yang, J.H., Pi, J.E., Kwon, O.S., Kim, G.H., Hwang, C.S., Bak, J.Y., and Yoon, S.M. (2015). Improvements in the bending performance and bias stability of flexible InGaZnO thin film transistors and optimum barrier structures for plastic poly (ethylene naphthalate) substrates. J. Mater. Chem. C *3*, 4779–4786. https://doi.org/10.1039/C5TC00048C.

Paskiewicz, D.M., Sichel-Tissot, R., Karapetrova, E., Stan, L., and Fong, D.D. (2015). Single-crystalline $SrRuO_3$ nanomembranes: a platform for flexible oxide electronics. Nano Lett. *16*, 534–542. https://doi.org/10.1021/acs.nanolett.5b04176.

Qi, Z., Jian, J., Huang, J., Tang, J., Wang, H., Pol, V.G., and Wang, H. (2018). $LiNi_{0.5}Mn_{0.3}Co_{0.2}O_2$/Au nanocomposite thin film cathode with enhanced electrochemical properties. Nano Energy *46*, 290–296. https://doi.org/10.1016/j.nanoen.2018.02.011.

Queraltó, A., Pérez del Pino, A., de la Mata, M., Arbiol, J., Obradors, X., and Puig, T. (2015). Ultrafast crystallization of $Ce_{0.9}Zr_{0.1}O_{2-y}$ epitaxial films on flexible technical substrates by pulsed laser irradiation of chemical solution derived precursor layers. Cryst. Growth Des. *15*, 1957–1967. https://doi.org/10.1021/acs.cgd.5b00115.

Roels, E., Terryn, S., Brancart, J., Sahraeeazartamar, F., Clemens, F., Van Assche, G., and Vanderborght, B. (2022). Self-healing sensorized soft robots. Materials Today Electronics *1*, 100003. https://doi.org/10.1016/j.mtelec.2022.100003.

Salles, P., Caño, I., Guzman, R., Dore, C., Mihi, A., Zhou, W., and Coll, M. (2021). Facile chemical route to prepare water soluble epitaxial $Sr_3Al_2O_6$ sacrificial layers for free-standing oxides. Adv. Mater. Interfaces *8*, 2001643. https://doi.org/10.1002/admi.202001643.

Sando, D., Yang, Y., Paillard, C., Dkhil, B., Bellaiche, L., and Nagarajan, V. (2018). Epitaxial ferroelectric oxide thin films for optical applications. Appl. Phys. Rev. *5*, 041108. https://doi.org/10.1063/1.5046559.

Shelton, C.T., and Gibbons, B.J. (2011). Epitaxial Pb(Zr, Ti)O_3 thin films on flexible substrates. J. Am. Ceram. Soc. *94*, 3223–3226. https://doi.org/10.1111/j.1551-2916.2011.04811.x.

Shen, L., Wu, L., Sheng, Q., Ma, C., Zhang, Y., Lu, L., Ma, J., Ma, J., Bian, J., Yang, Y., et al. (2017). Epitaxial lift-off of centimeter-scaled spinel ferrite oxide thin films for flexible electronics. Adv. Mater. *29*, 1702411. https://doi.org/10.1002/adma.201702411.

Shi, D.Q., Ko, R.K., Song, K.J., Chung, J.K., Ha, H.S., Kim, H.S., Moon, S.H., Yoo, S.I., and Park, C. (2005). Deposition of Y_2O_3 film on textured metal substrates for a single buffer layer of a YBCO coated conductor. Supercond. Sci. Technol. *18*, 561–565. https://doi.org/10.1088/0953-2048/18/4/029.

Shin, J., Goyal, A., Jesse, S., and Kim, D.H. (2009). Single-crystal-like, c-axis oriented $BaTiO_3$ thin films with high-performance on flexible metal templates for ferroelectric applications. Appl. Phys. Lett. *94*, 252903. https://doi.org/10.1063/1.3158955.

Son, D., Lee, J., Qiao, S., Ghaffari, R., Kim, J., Lee, J.E., Song, C., Kim, S.J., Lee, D.J., Jun, S.W., et al. (2014). Multifunctional wearable devices for diagnosis and therapy of movement disorders. Nat. Nanotechnol. *9*, 397–404. https://doi.org/10.1038/NNANO.2014.38.

Song, K., Noh, J., Jun, T., Jung, Y., Kang, H.Y., and Moon, J. (2010). Fully flexible solution-deposited ZnO thin-film transistors. Adv. Mater. *22*, 4308–4312. https://doi.org/10.1002/adma.201002163.

Sun, H., Luo, Z., Zhao, L., Liu, C., Ma, C., Lin, Y., Gao, G., Chen, Z., Bao, Z., Jin, X., et al. (2020a). $BiFeO_3$-based flexible ferroelectric memristors for neuromorphic pattern recognition. ACS Appl. Electron. Mater. *2*, 1081–1089. https://doi.org/10.1021/acsaelm.0c00094.

Sun, H.Y., Zhang, C., Song, J., Gu, J., Zhang, T., Zang, Y., Li, Y., Gu, Z., Wang, P., and Nie, Y. (2020b). Epitaxial optimization of atomically smooth $Sr_3Al_2O_6$ for freestanding perovskite films by molecular beam epitaxy. Thin Solid Films *697*, 137815. https://doi.org/10.1016/j.tsf.2020.137815.

Sun, X., Yuan, Y., Xiao, Y., Lu, Q., Yang, L., Chen, C., and Guo, Q. (2018). Three-dimensional strain engineering in epitaxial vertically aligned nanocomposite thin films with tunable magnetotransport properties. Biochem. Biophys. Res. Commun. *506*, 536–542. https://doi.org/10.1039/C8MH00216A.

Tak, B.R., Yang, M.M., Lai, Y.H., Chu, Y.H., Alexe, M., and Singh, R. (2020). Photovoltaic and flexible deep ultraviolet wavelength detector based on novel β-Ga_2O_3/muscovite heteroepitaxy. Sci. Rep. *10*, 16098. https://doi.org/10.1038/s41598-020-73112-1.

Tomov, R.I., Kursumovic, A., Majoros, M., Kang, D.J., Glowacki, B.A., and Evetts, J.E. (2002). Pulsed laser deposition of epitaxial $YBa_2Cu_3O_{7-y}$/oxide multilayers onto textured NiFe substrates for coated conductor applications. Supercond. Sci. Technol. *15*, 598–605. https://doi.org/10.1088/0953-2048/15/4/320.

Tsai, M., Zheng, Y., Lu, S., Zheng, J., Pan, H., Duan, C., Yu, P., Huang, R., and Chu, Y. (2021). Antiferroelectric anisotropy of epitaxial $PbHfO_3$ films for flexible energy storage. Adv. Funct. Mater. *31*, 2105060. https://doi.org/10.1002/adfm.202105060.

Tsakalakos, L., and Sands, T. (2000). Epitaxial ferroelectric (Pb, La)(Zr, Ti)O_3 thin films on stainless steel by excimer laser liftoff. Appl. Phys. Lett. *76*, 227–229. https://doi.org/10.1063/1.125710.

Wang, J., Neaton, J.B., Zheng, H., Nagarajan, V., Ogale, S.B., Liu, B., Viehland, D., Vaithyanathan, V., Schlom, D.G., Waghmare, U.V., et al. (2003). Epitaxial $BiFeO_3$ multiferroic thin film heterostructures. Science *299*, 1719–1722. https://doi.org/10.1126/science.1080615.

Wee, S.H., Huang, P.S., Lee, J.K., and Goyal, A. (2015). Heteroepitaxial Cu_2O thin film solar cell on metallic substrates. Sci. Rep. *5*, 16272. https://doi.org/10.1038/srep16272.

Xiong, J., Matias, V., Wang, H., Zhai, J.Y., Maiorov, B., Trugman, D., Tao, B.W., Li, Y.R., and Jia, Q.X. (2010). Much simplified ion-beam assisted deposition-TiN template for high-performance coated conductors. J. Appl. Phys. *108*, 083903. https://doi.org/10.1063/1.3499270.

Xiong, J., Matias, V., Tao, B.W., Li, Y.R., and Jia, Q.X. (2014). Ferroelectric and ferromagnetic properties of epitaxial $BiFeO_3$-$BiMnO_3$ films on ion-beam-assisted deposited TiN buffered flexible Hastelloy. J. Appl. Phys. *115*, 17D913. https://doi.org/10.1063/1.4869438.

Xue, Y., Zhang, Y.H., Zhang, F., Zhao, R.P., Wang, H., Xiong, J., and Tao, B.W. (2016). Growth of simplified buffer template on flexible metallic substrates for $YBa_2Cu_3O_{7-\delta}$ coated conductors. J. Alloys Compd. *673*, 47–53. https://doi.org/10.1016/j.jallcom.2016.02.175.

Yamamoto, Y., Harada, S., Yamamoto, D., Honda, W., Arie, T., Akita, S., and Takei, K. (2016). Printed multifunctional flexible device with an integrated motion sensor for health care monitoring. Sci.

Adv. *2*, e1601473. https://doi.org/10.1126/sciadv.1601473.

Yang, C., Han, Y., Qian, J., Lv, P., Lin, X., Huang, S., and Cheng, Z. (2019). Flexible, temperature-resistant, and fatigue-free ferroelectric memory based on $Bi(Fe_{0.93}Mn_{0.05}Ti_{0.02})O_3$ thin film. ACS Appl. Mater. Interfaces *11*, 12647–12655. https://doi.org/10.1021/acsami.9b01464.

Ye, L., Zhang, D., Lu, J., Xu, S., Xu, R., Fan, J., Tang, R., Wang, H., Guo, H., Li, W., and Yang, H. (2022). Epitaxial (110)-oriented $La_{0.7}Sr_{0.3}MnO_3$ film directly on flexible mica substrate. J. Phys. D Appl. Phys. *55*, 224002. https://doi.org/10.1088/1361-6463/ac570d.

Yen, M., Lai, Y., Kuo, C., Chen, C., Chang, C., and Chu, Y. (2020). Mechanical modulation of colossal magnetoresistance in flexible epitaxial perovskite manganite. Adv. Funct. Mater. *30*, 2004597. https://doi.org/10.1002/adfm.202004597.

Zhang, B., Huang, J., Rutherford, B., Lu, P., Misra, S., Kalaswad, M., He, Z., Gao, X., Sun, X., Li, L., and Wang, H. (2020a). Tunable, room-temperature multiferroic Fe-$BaTiO_3$ vertically aligned nanocomposites with perpendicular magnetic anisotropy. Materials Today Nano *11*, 100083. https://doi.org/10.1016/j.mtnano.2020.100083.

Zhang, B., Yun, C., and MacManus-Driscoll, J.L. (2021). High yield transfer of clean large-area epitaxial oxide thin films. Nano-Micro Lett. *13*, 39. https://doi.org/10.1007/s40820-020-00573-4.

Zhang, J., Zhang, W., Cheng, H.M., and Silva, S.R.P. (2020b). Critical review of recent progress of flexible perovskite solar cells. Mater. Today *39*, 66–88. https://doi.org/10.1016/j.mattod.2020.05.002.

Zhang, Y., Shen, L., Liu, M., Li, X., Lu, X., Lu, L., Ma, C., You, C., Chen, A., Huang, C., et al. (2017). Flexible quasi-two-dimensional $CoFe_2O_4$ epitaxial thin films for continuous strain tuning of magnetic properties. ACS Nano *11*, 8002–8009. https://doi.org/10.1021/acsnano.7b02637.

Zheng, M., Sun, H., and Kwok, K.W. (2019a). Mechanically controlled reversible photoluminescence response in all-inorganic flexible transparent ferroelectric/mica heterostructures. NPG Asia Mater. *11*, 52. https://doi.org/10.1038/s41427-019-0153-7.

Zheng, W.C., Zheng, D.X., Wang, Y.C., Jin, C., and Bai, H.L. (2018). Uniaxial strain tuning of the Verwey transition in flexible Fe_3O_4/muscovite epitaxial heterostructures. Appl. Phys. Lett. *113*, 142403. https://doi.org/10.1063/1.5050546.

Zheng, W.C., Zheng, D., Wang, Y., Li, D., Jin, C., and Bai, H. (2019b). Flexible $Fe_3O_4/BiFeO_3$ multiferroic heterostructures with uniaxial strain control of exchange bias. J. Magn. Magn Mater. *481*, 227–233. https://doi.org/10.1016/j.jmmm.2019.02.068.

Zheng, Y., Wang, B., and Woo, C.H. (2008). Piezoelectric bending response and switching behavior of ferroelectric/paraelectric bilayers. Acta Mater. *56*, 479–488. https://doi.org/10.1016/j.actamat.2007.10.011.